Light-trapping for room temperature Bose-Einstein condensation in InGaAs quantum wells

Pranai Vasudev,[1,*] **Jian-Hua Jiang,**[1] **and Sajeev John**[1]

[1]*Department of Physics, University of Toronto, Toronto, Ontario, Canada M5S 1A7*

[*]*pranai.vasudev@mail.utoronto.ca*

Abstract: We demonstrate the possibility of room-temperature, thermal equilibrium Bose-Einstein condensation (BEC) of exciton-polaritons in a multiple quantum well (QW) system composed of InGaAs quantum wells surrounded by InP barriers, allowing for the emission of light near telecommunication wavelengths. The QWs are embedded in a cavity consisting of double slanted pore (SP2) photonic crystals composed of InP. We consider exciton-polaritons that result from the strong coupling between the multiple quantum well excitons and photons in the lowest planar guided mode within the photonic band gap (PBG) of the photonic crystal cavity. The collective coupling of three QWs results in a vacuum Rabi splitting of 3% of the bare exciton recombination energy. Due to the full three-dimensional PBG exhibited by the SP2 photonic crystal (16% gap to mid-gap frequency ratio), the radiative decay of polaritons is eliminated in all directions. Due to the short exciton-phonon scattering time in InGaAs quantum wells of 0.5 ps and the exciton non-radiative decay time of 200 ps at room temperature, polaritons can achieve thermal equilibrium with the host lattice to form an equilibrium BEC. Using a SP2 photonic crystal with a lattice constant of $a = 516$ nm, a unit cell height of $\sqrt{2}a = 730$ nm and a pore radius of $0.305a = 157$ nm, light in the lowest planar guided mode is strongly localized in the central slab layer. The central slab layer consists of 3 nm InGaAs quantum wells with 7 nm InP barriers, in which excitons have a recombination energy of 0.944 eV, a binding energy of 7 meV and a Bohr radius of $a_B = 10$ nm. We take the exciton recombination energy to be detuned 35 meV above the lowest guided photonic mode so that an exciton-polariton has a photonic fraction of approximately 97% per QW. This increases the energy range of small-effective-mass photonlike states and increases the critical temperature for the onset of a Bose-Einstein condensate. With three quantum wells in the central slab layer, the strong light confinement results in light-matter coupling strength of $\hbar\Omega = 13.7$ meV. Assuming an exciton density per QW of $(15a_B)^{-2}$, well below the saturation density, in a 2-D box-trap with a side length of 10 to 500 μm, we predict thermal equilibrium Bose-Einstein condensation well above room temperature.

OCIS codes: (270.0270) Quantum Optics; (250.0250) Optoelectronics.

#260856 Received 17 Mar 2016; revised 13 May 2016; accepted 8 Jun 2016; published 14 Jun 2016

References and links

1. H.Haug and S. Koch, *Quantum Theory of the Optical and Electronic Properties of Semiconductors* (World Scientific Publishing, 2004).
2. D. A. B. Miller, "Optical physics of quantum wells," in *Quantum Dynamics of Simple Systems*, G. Oppo, S. Barnett, E. Riis and M. Wilkinson eds. (Institute of Physics, 1996).
3. J. Kasprzak, M. Richard, S. Kundermann, A. Baas, P. Jeambrun, J. M. J. Keeling, F. M. Marchetti, M. H. Szymańska, R. André, J. L. Staehli, V. Savona, P. B. Littlewood, B. Deveaud, and L. S. Dang, "BoseEinstein condensation of exciton polaritons," Nature **443**, 409–414 (2006).
4. R. Balili, V. Hartwell, D. Snoke, L. Pfeiffer, and K. West, "Bose-Einstein condensation of microcavity polaritons in a trap," Science **316**, 1007–1010 (2007).
5. J. Kasprzak, D. D. Solnyshkov, R. André, L. S. Dang, and G. Malpuech, "Formation of an exciton polariton condensate: thermodynamic versus kinetic regimes," Phys. Rev. Lett. **82**(14) 146404 (2008).
6. H. Deng, H. Haug, and Y. Yamamoto, "Exciton-polariton Bose-Einstein condensation," Rev. Mod. Phys. **82**(2), 1489–1537 (2010).
7. I. Carusotto and C. Ciuti, "Quantum fluids of light," Rev. Mod. Phys. **85**(1), 299–366 (2013).
8. T. Byrnes, N. Y. Kim, and Y. Yamamoto, "Exciton-polariton condensates," Nat. Phys. **10**(11), 803–813 (2014).
9. H. Deng, D. Press, S. Götzinger, R. Hey, K. H. Ploog, and Y. Yamamoto, "Quantum degenerate exciton-polaritons in thermal equilibrium," Phys. Rev. Lett. **97**(14), 146402 (2006).
10. S.-K. Chang, A. V. Nurmikko, J.-W. Wu, L. A. Kolodziejski, and R. L. Gunshor, "Band offsets and excitons in CdTe/(Cd, Mn) Te quantum wells," Phys. Rev. B **37**(3), 1191–1198 (1988).
11. R. C. Miller, D. A. Kleinman, W. T. Tsang, and A. C. Gossard, "Observation of the excited level of excitons in GaAs quantum wells," Phys. Rev. B **24**(2), 1134–1136 (1981).
12. H. Deng, G. Weihs, D. Snoke, J. Bloch, and Y. Yamamoto, "Polariton lasing vs. photon lasing in a semiconductor microcavity," Proc. Nat. Acad. Sci. **100**(26), 15318–15323 (2003).
13. B. Nelsen, G. Liu, M. Steger, D. W. Snoke, R. Balili, K. West, and L. Pfeiffer, "Dissipationless flow and sharp threshold of a polariton condensate with long lifetime," Phys. Rev. X **3**(4), 041015 (2013).
14. A. Honold, L. Schultheis, J. Kuhl, and C. W. Tu, "Collision broadening of two-dimensional excitons in a GaAs single quantum well," Phys. Rev. B **40**(9), 6442–6445 (1989).
15. M. Zamfirescu, A. Kavokin, B. Gil, G. Malpuech, and M. Kaliteevski, "ZnO as a material mostly adapted for realization of room-temperature polariton lasers," Phys. Rev. B **65**(16), 161205 (2002).
16. R. Schmidt-Grund, B. Rheinländer, C. Czkalla, G. Benndorf, H. Hochmuth, M. Lorenz, and M. Grundmann, "Excitonpolariton formation at room temperature in a planar ZnO resonator structure," Appl. Phys. B **93**(2), 331–337 (2008).
17. F. Li, L. Orosz, O. Kamoun, S. Bouchoule, C. Brimont, P. Disseix, T. Guillet, X. Lafosse, M. Leroux, J. Leymarie, M. Mexis, M. Mihailovic, G. Patriarche, F. Réveret, D. Solnyshkov, J. Zuniga-Perez, and G. Malpuech, "From excitonic to photonic polariton condensate in a ZnO-Based microcavity," Phys. Rev. Lett. **110**(19), 196406 (2013).
18. A. Das, J. Heo, A. Bayraktaroglu, W. Guo, T.-K. Ng, J. Phillips, B. S. Ooi, and P. Bhattacharya, "Room temperature strong coupling effects from single ZnO nanowire microcavity," Opt. Express **20**(11), 11830–11837 (2012).
19. L. Orosz, F. Réveret, F. Médard, P. Disseix, J. Leymarie, M. Mihailovic, D. Solnyshkov, G. Malpuech, J. Zuniga-Pérez, and G. Malpuech, "LO-phonon assisted polariton lasing in a ZnO based microcavity," Phys. Rev. B **85**(12), 121201 (2012).
20. R. Johne, D. Solnyshkov, and G. Malpuech, "Theory of exciton-polariton lasing at room temperature in ZnO microcavities," Appl. Phys. Lett. **93**(21), 211105 (2008).
21. S. Christopoulos, G. Baldassari Höger von Högersthal, A. J. D. Grundy, P. G. Lagoudakis, A. V. Kavokin, J. J. Baumberg, G. Christmann, R. Butté, E. Feltin, J.-F. Carlin, and N. Grandjean, "Room-temperature polariton lasing in semiconductor microcavities," Phys. Rev. Lett. **98**(12), 126405 (2007).
22. N. Antoine-Vincent, F. Natali, D. Byrne, A. Vasson, P. Disseix, J. Leymarie, M. Leroux, F. Semond, and J. Massies, "Observation of Rabi splitting in a bulk GaN microcavity grown on silicon," Phys. Rev. B **68**(15), 153313 (2003).
23. M. Leroux, N. Grandjean, M. Laügt, J. Massies, B. gil, P. Lefebvre, and P. Bigenwald, "Quantum confined Stark effect due to built-in internal polarization fields in (Al,Ga)N/GaN quantum wells," Phys. Rev. B **58**(20), R13371 (1998).
24. S. Kéna-Cohen and S. R. Forrest, "Room Temperature Polariton Lasing in an Organic Single Crystal Microcavity," Nat. Photonics **4**(6), 371–375 (2010).
25. J. D. Plumhof , T. Stöferle, L. Mai, U. Scherf, and R. F. Mahrt, "Room-temperature BoseEinstein condensation of cavity excitonpolaritons in a polymer," Nat. Mat. **13**(3), 247–252 (2014).
26. C. P. Dietrich, A. Steude, L. Tropf, M. Schubert, N. M. Kronenberg, K. Ostermann, S. Höfling, and M. C. Gather, "An exciton-polariton laser based on biologically produced fluorescent protein," arXiv:1601.06983 (2016).
27. D. M. Coles, P. Michetti, C. Clark, W. C. Tsoi, A. M. Adawi, J.-S. Kim, and D. G. Lidzey, "Vibrationally assisted polariton-relaxation processes in strongly coupled organic-semiconductor microcavities," Adv. Functional Mater.

#260856 Received 17 Mar 2016; revised 13 May 2016; accepted 8 Jun 2016; published 14 Jun 2016

21(19), 3691–3696 (2011).
28. M. Litinskaya, P. Reineker, and V. M. Agranovich, "Fast polariton relaxation in strongly coupled organic microcavities," J. Luminescence **110**(4), 364–372 (2004).
29. J. Klaers, J. Schmitt, F. Vewinger, and M. Weitz, "BoseEinstein condensation of photons in an optical microcavity," Nature **468**(7323), 545–548 (2010).
30. J. Klaers, J. Schmitt, T. Damm, F. Vewinger, and M. Weitz, "Statistical physics of Bose-Einstein-condensed light in a dye microcavity," Phys. Rev. Lett. **108**(16), 160403 (2012).
31. J. Klaers, F. Vewinger, and M. Weitz, "Thermalisation of a two-dimensional photonic gas in a 'white-wall' photon box," Nat. Phys. **6**(7), 512–515 (2010).
32. J. Schmitt, T. Damm, D. Dung, F. Vewinger, J. Klaers, and M. Weitz, "Observation of grand-canonical number statistics in a photon Bose-Einstein condensate," Phys. Rev. Lett. **112**(3), 030401 (2014).
33. K. B. Davis, M. O. Mewes, M. R. Andrews, N. J. Van Druten, D. S. Durfee, D. M. Kurn, and W. Ketterle, "Bose-Einstein condensation in a gas of sodium atoms," Phys. Rev. Lett. **75**(22), 3969–3973 (1995).
34. V. V. Kocharovsky, V. V. Kocharovsky, M. Holthaus, C. H. Raymond Ooi, A. Svidzinsky, W. Ketterle, and M. O. Scully, "Fluctuations in Ideal and Interacting Bose-Einstein Condensates: From the Laser Phase Transition Analogy to Squeezed States and Bogoliubov Quasiparticles," Adv. Atomic, Molecular Opt. Phys. **53**(6), 291–411 (2006).
35. M. Steger, C. Gautham, D. W. Snoke, L. Pfeiffer, and K. West, "Slow reflection and two-photon generation of microcavity exciton-polaritons," Optica **2**(1), 1–5 (2015).
36. S. John, "Strong localization of photons in certain disordered dielectric superlattices," Phys. Rev. Lett. **58**(23), 2486–2489 (1987).
37. E. Yablonovitch, "Inhibited spontaneous emission in solid-state physics and electronics," Phys. Rev. Lett. **58**(20), 2059–2062 (1987).
38. J. D. Joannopoulos, S. G. Johnson, J. N. Winn, and R. D. Meade, *Photonic Crystals: Molding the Flow of Light* (Princeton University, 2008).
39. Y. Takahashi, H. Hagino, Y. Tanaka, B.-S. Song, T. Asano, and S. Noda, "High-Q photonic nanocavity with a 2-ns photon lifetime," Opt. Express **15**(25), 17206–17213 (2007).
40. G. S. Buller, S. J. Fancey, J. S. Massa, A. C. Walker, S. Cova, and A. Lacaita, "Time-resolved photoluminescence measurements of InGaAs/ InP multiple-quantum-well structures at 1.3-μm wavelengths by use of germanium single-photon avalanche photodiodes," Appl. Opt. **25**(6), 916–921 (1996).
41. O. Toader and S. John, "Slanted-pore photonic band-gap materials," Phys. Rev. E **71**(3), 036605 (2005)
42. O. Madelung, *Semiconductors: Data Handbook 3*rd *Edition* (Springer-Verlag, 2004).
43. M. S. Skolnick, P. R. Tapster, S. J. Bass, A. D. Pitt, N. Apsley, and S. P. Aldred, "Investigation of InGaAs-InP quantum wells by optical spectroscopy," Semicond. Sci. Techn. **1**(1), 29–40 (1986).
44. D. J. Westland, A. M. Fox, A. C. Maciel, J. F. Ryan, M. D. Scott, J. I. Davies, and J. R. Riffat, "Optical studies of excitons in $Ga_{0.47}In_{0.53}As/InP$ multiple quantum wells," Appl. Phys. Lett. **50**(13), 839–841 (1987).
45. J.-H. Jiang and S. John, "Photonic crystal architecture for room-temperature equilibrium Bose-Einstein condensation of exciton polaritons," Phys. Rev. X **4**(03), 031025 (2014).
46. J.-H. Jiang and S. John, "Photonic architectures for equilibrium high-temperature Bose-Einstein condensation in dichalcogenide monolayers," Nat. Sci. Rep. **4**(7432), 1–6 (2014).
47. S. Takahashi, K. Suzuki, M. Okano, M. Imada, T. Nakamori, Y. Ota, K. Ishizaki, and S. Noda, "Direct creation of three-dimensional photonic crystals by a top-down approach," Nat. Mat. **8**(9), 721–725 (2009).
48. N. Ttreault, G. Freymann, M. Deubel, M. Hermatschweiler, F. Prez-Willard, S. John, M. Wegener, and G. A. Ozin, "New route to three-dimensional photonic bandgap materials: silicon double inversion of polymer templates," Adv. Mater. **18**(4), 457–460 (2006).
49. S. Juodkazis, L. Rosa, S. Bauerdick, L. Peto, R. E.-Ganainy, and S. John, "Sculpturing of photonic crystals by ion beam lithography: towards complete photonic bandgap at visible wavelengths," Opt. Express **19**(7), 5802–5810 (2011).
50. M. Deubel, M. Wegener, A. Kaso, and S. John, "Direct laser writing and characterization of "slanted pore" photonic crystals," Appl. Phys. Lett. **85**(11) 1895–1897 (2004).
51. S. G. Johnson and J. D. Joannopoulos, "Block-iterative frequency-domain methods for Maxwell's equations in a planewave basis," Opt. Express **8**(3), 173–190 (2001).
52. S. Yang and S. John, "Exciton dressing and capture by a photonic band edge," Phys. Rev. B **75**(23), 235332 (2007).
53. E. Hanamura and H. Haug, "Condensation effects of excitons," Phys. Lett. **33**(4), 209–284 (1977).
54. Y. Yamamoto, F. Tassone, and H. Cao, *Semiconductor Cavity Quantum Electrodynamics* (Springer-Verlag, 2000).
55. I. Vurgaftman, J. R. Meyer, and L. R. Ram-Mohan, "Band parameters for IIIV compound semiconductors and their alloys," J. Appl. Phys. **89**(11), 5815–5875 (2001).
56. M. Vetterli, J. Kovacevic, and V. K. Goyal, *Foundations of Signal Processing* (Cambridge University, 2014).
57. S. Schmitt-Rink, D. S. Chemla, and D. A. B. Miller, "Theory of transient excitonic optical nonlinearities in semiconductor quantum-well structures," Phys. Rev. B **32**(10), 6601–6609 (1985).
58. P. Harrison, *Quantum Wells, Wires and Dots* (John Wiley and Sons, 2005).

#260856 Received 17 Mar 2016; revised 13 May 2016; accepted 8 Jun 2016; published 14 Jun 2016

59. T. Ishikawa and J. E. Bowers, "Band lineup and in-plane effective mass of InGaAsP or InGaAlAs on InP strained-layer quantum well," IEEE J. Quantum Electron. **30**(2), 562–570 (1994).
60. E. Zielinski, H. Schweizer, K. Streubel, H. eisele, and G. Weimann, "Excitonic transitions and exciton damping processes in InGaAs/InP," J. Appl. Phys. **59**(6), 2196–2204 (1986).
61. Y. Kawaguchi and H. Asahi, "High-temperature observation of heavy-hole and light-hole excitons in InGaAs/InP multiple quantum well structures grown by metalorganic molecular beam epitaxy," Appl. Phys. Lett. **50**(18), 1243–1245 (1987).
62. K. Tai, J. Hegarty, and W. T. Tsang, "Observation of optical Stark effect in InGaAs/InP multiple quantum wells," Appl. Phys. Lett. **51**(3), 152–154 (1987).
63. D. W. Snoke and J. P. Wolfe, "Population dynamics of a Bose gas near saturation," Phys. Rev. B **39**(7), 4030–4037 (1989).
64. F. Tassone and Y. Yamamoto, "Exciton-exciton scattering dynamics in a semiconductor microcavity and stimulated scattering into polaritons," Phys. Rev. B **59**(16), 10830–10842 (1999).
65. M. S. Skolnick, K. J. Nash, M. K. Saker, S. J. Bass, P.A. Claxton, and J. S. Roberts, "Free-carrier effects on luminescence linewidths in quantum wells," Appl. Phys. Lett. **50**(26), 1885–1887 (1987).
66. B.-S. Song, S. Noda, T. Asano, and Y. Akahane, "Ultra-high-Q photonic double-heterostructure nanocavity," Nat. Mat. **4**(3), 207–210 (2005).
67. N. D. Mermin and H. Wagner, "Absence of ferromagnetism or antiferromagnetism in one- or two-dimensional isotropic Heisenberg models," Phys. Rev. Lett. **17**(22), 1133–1136 (1966).
68. P. Hohenberg, "Existence of long-range order in one and two dimensions," Phys. Rev. **158**(2), 383–386 (1967).
69. É. B. Sonin, "Quantization of the magnetic flux of superconducting rings and Bose condensation," Sov. Phys. JETP **29**(3), 520–525 (1969).
70. D. S. Petrov, D. M. Gangardt, and G. V. Shlyapnikov, "Low-dimensional trapped gases," J. Phys. IV France **116**, 5–44 (2004).
71. S. Ogawa, M. Imada, S. Yoshimoto, M. Okano, and S. Noda, "Control of light emission by 3D photonic crystals," Science **305**(5681), 227–229 (2004).
72. S. Noda, M. Fujita and T. Asano, "Spontaneous-emission control by photonic crystals and nanocavities," Nat. Photonics **1**(8), 449–458 (2007).
73. W. Ketterle and N. J. van Druten, "Bose-Einstein condensation of a finite number of particles trapped in any-dimensional space," Phys. Rev. A **54**(1), 656–660 (1996).
74. O. Penrose and L. Onsager, "Bose-Einstein condensation and liquid helium," Phys. Rev. **104**(3), 576–584 (1956).
75. S. Schmitt-Rink, D. S. Chemla, and D. A. B. Miller, "Linear and nonlinear optical properties of semiconductor quantum wells," Adv. Phys. **38**(2), 89–188 (1989).
76. G. Livescu, D. A. B. Miller, D. S. Chemla, M. Ramaswamy, T. Y. Chang, N. Sauer, A. C. Goassard, and J. H. English, "Free carrier and many-body effects in absorption spectra of modulation-doped quantum wells," IEEE J. Quantum Electron. **24**(8), 1677–1689 (1988).
77. V. Savona, L. C. Andreani, P. Schwendimann, and A. Quattropani, "Quantum well excitons in semiconductor microcavities: Unified treatment of weak and strong coupling regimes," Solid State Commun. **93**(9), 733–739 (1995).

1. Introduction

With increasingly advanced fabrication technologies, semiconductor nanostructures are becoming more and more important in the study of cavity quantum electrodynamics and strong light-matter interaction. Elementary excitations in semiconductor crystals, known as excitons, have been extensively studied in the literature [1]. The confinement of excitons to regions of low-dimensionality, such as two-dimensional quantum wells or "zero-dimensional" quantum dots, is of particular interest because the quantum confinement can drastically alter the electronic density of states [1, 2]. In the case of quantum wells (QWs), the use of an optical cavity to confine light to the QW region allows for strong exciton-photon coupling and the formation of exciton-polaritons. These exciton-polaritons are associated with normal mode splitting into a lower and upper polariton branch and they behave as bosonic quasi-particles (for small densities) with a "half-light" and "half-matter" nature [3–8]. The strong photon-exciton coupling causes the lower polaritons to have a sharp minimum in their dispersion. The depth of this minimum, referred to as the dispersion depth, is governed by the exciton-photon detuning and the light-matter coupling strength. The dispersion depth plays a central role in exciton-polariton Bose-Einstein condensation (BEC) physics. For deeper dispersion depths, the polaritons tend

#260856 Received 17 Mar 2016; revised 13 May 2016; accepted 8 Jun 2016; published 14 Jun 2016

to occupy the low energy photonlike states that have smaller effective masses as opposed to the higher energy excitonlike states with electron-like effective masses. At the minimum of the lower polariton dispersion, the strong light-matter coupling endows the polaritons with an effective mass on the order of 10^{-5} of the bare electron mass. Due to their small effective mass and their bosonic nature, exciton-polaritons in the lower branch are a candidate for high-temperature BEC. Roughly speaking, a BEC of exciton-polaritons occurs for a sufficiently large polariton density (at a fixed temperature) or for a sufficiently small temperature (at a fixed density) such that the thermal de Broglie wavelength $h/\sqrt{2\pi m k_B T}$ is on the order of the interparticle spacing. At this critical density (or temperature), macroscopic occupation of the polariton ground state triggers a BEC.

To date, most exciton-polariton Bose-Einstein condensation (BEC) experiments have been conducted in semiconductor microcavities composed of Fabry-Perot etalons, with quantum wells placed in the cavity where the peak of the field intensity occurs. Typically, only quasi-equilibrium condensates are obtained because the condensate has almost reached thermal equilibrium with itself, but not with the host lattice [5, 9]. Quasi-equilibrium occurs when the relaxation kinetics for the polaritons act on the time scale of the polariton lifetime. The kinetics act fast enough for the condensate to almost reach self-equilibrium, but not fast enough for the polaritons to fully thermalize with the host lattice. For condensates in quasi-equilibrium, an effective temperature T_{eff} can be assigned where $T_{\text{eff}} > T_{\text{lat}}$ and T_{lat} is the lattice temperature. As the condensates decay, they are replenished by a pumping laser. In experiments in Fabry-Perot type cavities, T_{eff} is on the order of 10 K and the apparatus requires cooling by liquid helium.

Photonic band gap (PBG) materials offer three significant advantages over 1D Fabry-Perot cavities: (i) the 3D PBG architecture involves a higher dielectric contrast, enabling much smaller mode volume for trapped light and stronger exciton-photon coupling strength. (ii) The 3D PBG architecture enables breaking of the optical field polarization degeneracy in the plane of the quantum well. This leads to a doubling of the polariton density relevant to BEC for a given overall exciton density in the QW. For a 1D Fabry-Perot cavity, the polariton density is divided between two degenerate ground states. (iii) The 3D PBG eliminates radiative decay of polaritons to the extent desired in all spatial directions from a small ($\sim$10 micron scale) trapped condensate. In a 1D Fabry-Perot cavity, a trapped condensate contains wave vector components that couple to degenerate off-normal optical modes leading to picosecond radiative decay of polaritons, even when the cavity quality factor is high. In contrast, the 3D PBG facilitates a long lifetime of the polariton BEC.

Indium-phosphide based PBG materials surrounding InGaAs quantum wells offer the opportunity for light emission from a polariton condensate at near-telecommunication wavelengths. In such light emission, quantum correlations between polaritons can be mapped onto quantum correlations of emitted photons. A source of non-classical states of light of this type may have applications in a futuristic quantum communication network.

Quasi-equilibrium BEC of exciton-polaritons has been experimentally achieved in CdTe-based architectures [3]. Here, 16 CdTe-based QWs were embedded in a Fabry-Perot type cavity. A collective exciton-photon coupling $\hbar\Omega = 13$ meV and an effective temperature of $T_{\text{eff}} \simeq 19$ K for quasi-equilibrium condensation was reported. CdTe-based architectures can be excited to high polariton densities, due to the relatively small excitonic Bohr radius (4.5 nm [10]). This is smaller than the exciton radius in GaAs-based systems (10 nm [11]), where similar densities would cause dissociation by exciton-exciton collisions. An advantage of CdTe-based QWs is that they can be fabricated to very high crystalline quality by molecular beam epitaxy [10]. The resulting inhomogeneous broadening of the exciton emission line (1 meV [10]) is small compared to the light-matter coupling strength, and consequently, the lower polariton's dispersion depth remains relatively intact. However, the exciton recombination wavelength in

#260856 Received 17 Mar 2016; revised 13 May 2016; accepted 8 Jun 2016; published 14 Jun 2016

CdTe of 750 nm [10] is far from the 1500 nm used in telecommunications.

Quasi-equilibrium BEC of exciton-polaritons has also been reported in GaAs-based architectures. Here, 12 GaAs-based QWs in a Fabry-Perot type cavity provided a collective exciton-photon coupling of 6 meV and a quasi-equilibrium condensate at $T_{\text{eff}} \simeq 50$ K while the lattice temperature was 4 K [4, 12, 13]. Here again, precise fabrication technologies reduce the inhomogeneous broadening of the exciton emission line to 1 meV [14]. The large exciton Bohr radius of 10 nm [11] limits the stable polariton densities possible in GaAs-based QWs. The emission wavelength in GaAs-based QWs is 780 nm [11].

Polariton lasing [15] and room-temperature metastable polariton condensates [16, 17] have been suggested in ZnO-based architectures. The metastable condensates [16,17], however, cannot be fit by a Bose distribution at a temperature T_{eff} [5], but the lattice is held at room temperature. Very large exciton-photon coupling of $\hbar\Omega = 60$ meV [15, 16] and $\hbar\Omega = 95$ meV [17] have been reported. There have also been reports of strong coupling ($\hbar\Omega = 100$ meV) at room temperature between excitons in ZnO nanowires embedded in a Fabry-Perot cavity [18]. Unfortunately, the polariton lifetime in ZnO is approximately 0.1 ps [19] and the polariton-phonon scattering time is approximately 2 ps [15]. While the exciton Bohr radius in ZnO is only 1.8 nm [16], the small excitons are very sensitive to local crystalline disorder, leading to a large inhomogeneous broadening value of 50 meV [16, 20]. As a result, the lower polariton dispersion is smeared. In ZnO based architectures, light emission occurs at 365 nm [15] very far from telecommunication wavelengths.

Claims of room-temperature polariton lasing from metastable polariton condensates have likewise been made in GaN-based architectures. Here, an effective temperature is not assigned to the condensate, while the host lattice is held at 300 K [21]. The authors report large exciton-photon coupling of approximately 25 meV. However, these condensates are not in thermal equilibrium or even quasi-equilibrium since the polariton lifetime is on the order of 1 ps and the thermalization time is the same [21]. In GaN, the small excitonic Bohr radius of 3.5 nm [21] allows for higher polariton densities than in GaAs. As in the case of ZnO, these small excitons are very sensitive to crystalline disorder, resulting in a large inhomogeneous broadening (30 meV [22, 23]) of the exciton emission line. This inhomogeneous broadening significantly smears the lower polariton's dispersion depth. Light emission from GaN QWs occurs at about 365 nm [21].

There have also been claims of polariton lasing and BEC in organic-based systems. For example, Ref. [24] reports polariton lasing from an anthracene microcavity at room temperature with an emission wavelength of 422 nm. In Ref. [25], the authors claim (non-equilibrium) BEC of exciton-polaritons in a ladder-conjugated polymer active layer at room temperature, with an emission wavelength of 475 nm. There have also been reports of polariton lasing from biologically active protein-based materials [26]. Organic systems are advantageous for forming polariton condensates since the relevant electronic excitations are Frenkel excitons with approximately eV scale binding energies [24] and very large light-matter coupling strengths of $\hbar\Omega = 75$ meV [25]. Due to the small excitons, organic systems have a significantly increased saturation density. However, these systems have drawbacks that the optical cavities are often low quality, resulting in picosecond polariton lifetimes [27]. Moreover, relaxation of reservoir excitons into the LP branch is slow with the relaxation times ranging from 20 ps to 100 ps [24, 28]. This suggests that the polaritons in these systems cannot reach thermal equilibrium to form a true BEC.

There have also been claims of BECs of photons in cavities composed of curved mirrors filled with dyes [29]. The authors claim that the dye molecules act as a thermal reservoir and the photons thermalize to the temperature of the dye by scattering multiple times from the dye molecules [30]. These experiments exhibit characteristics of BECs such as a thermal distribu-

#260856 Received 17 Mar 2016; revised 13 May 2016; accepted 8 Jun 2016; published 14 Jun 2016

tion in the photon spectrum and spatial narrowing above a certain pumping threshold [31]. However, the condensates exhibit fluctuations in the number of particles in the ground state on the order of N_0 where N_0 is the number of photons in the ground state [32]. This is unlike standard BECs in atomic systems [33] where the fluctuations are on the the order of $\sqrt{N_0}$ [34].

A fundamental limitation in all the microcavity polariton experiments to date is that strong coupling promotes rapid radiative decay of excitons and the condensates created in 1D Fabry-Perot cavities are too short lived to obtain thermal equilibrium. Even with high-quality factor cavities, the polariton lifetime is on the order of 200 ps [13, 35] due to the strong coupling to extraneous optical modes. The thermalization time is possibly on the same order [9]. In optical cavities based on photonic band gap materials [36–38], strong coupling to a desired mode is achieved without rapid radiative decay into extraneous modes, irrespective of the condensate trapping area. Moreover, PBG cavities confine light to the QW regions more strongly than Fabry-Perot type cavities. This is because in the PBG materials, the photonic crystal is air filled, allowing for a stonger dielectric contrast than in Fabry-Perot type cavities, where the dielectric contrast is between two III-V semiconductors [3, 4]. This stronger light confinement enhances the photon-exciton coupling in the QW regions. At the same time, the full three-dimensional band gap inhibits the radiative decay of exciton-polaritons in all directions, increasing the exciton-polariton lifetime, possibly to the order of nanoseconds [39]. Non-radiative decay processes that may act on a 100 ps time scale [40], leave the exciton-polaritons enough time to thermalize with the host lattice.

In this article, we consider the thermal equilibrium room-temperature BEC of exciton-polaritons in $In_{0.53}Ga_{0.47}As$ (which we simply refer to as InGaAs) QWs with InP barriers in an optical cavity composed of double slanted pore InP photonic crystals [41]. We consider a structure composed with two to three QWs sandwiched between the slanted pore crystals, as depicted in Fig. 1(a). InGaAs wells surrounded by InP allow for the emission of light near the telecommunications band of $1.5\,\mu$m. Blended in the specified proportions, InGaAs has a direct band gap of 0.8215 eV and InP has a direct band gap of 1.42 eV [42]. The lateral confinement of the excitons induced by the QW causes electrons and holes to occupy subbands in the InGaAs QWs. In 3 nm InGaAs wells surrounded by 7 nm InP barriers, the heavy hole-conduction electron exciton has a recombination energy of 0.944 eV, corresponding to an optical wavelength of $1.3\,\mu$m. Another advantage to using InGaAs-based quantum wells is that there exists well developed fabrication techniques for InGaAs/InP QWs such as metalorganic chemical vapor deposition [43]. With these precise fabrication technologies, the inhomogeneous broadening of the exciton's emission line is on the order of 1 meV [44]. This ensures that the lower polariton's dispersion depth remains unsmeared.

There are several advantages to the slanted pore PBG architecture for the optical cavity. First, slanted pore photonic crystals exhibit a large three dimensional band gap. Our InP slanted pore crystal with dielectric constant 10.88 [42] and pore radius of $0.305a$ (where a is x-y the lattice constant as shown in Fig. 1(a)), exhibits a 3D PBG with gap-to-midgap ratio of 16%. This is a larger PBG than possible with woodpile crystals [45, 46], and leads to stronger exciton-photon coupling as well as better protection for the resulting polariton from radiative decay. The second significant advantage of the slanted pore architecture is that the x-y symmetry in the plane of the quantum wells is broken. By breaking the x-y symmetry, the two-fold degeneracy of the exciton-polaritons' ground state that exists in Fabry-Perot based and woodpile based cavities is lifted [46]. This allows for an increase in the effective polariton density available for BEC by a factor of two [46]. Despite the seemingly complex architecture, there exist technologies to fabricate slanted pore photonic crystals. For example, in Ref. [47], the authors demonstrate a double-angled etching method to fabricate woodpile photonic crystals designed to operate in the telecommunications band. They indicate that this method could also be used to fabricate

#260856 Received 17 Mar 2016; revised 13 May 2016; accepted 8 Jun 2016; published 14 Jun 2016

slanted pore crystals. They furthermore suggest that light-emitting quantum well layers could be fused with the photonic crystal using wafer bonding technology. Ref. [48] demonstrates the fabrication of woodpile photonic crystals with a band gap in the visible frequencies, using a silicon double inversion of polymer template technique. The authors indicate that this technique is also suitable for the fabrication of slanted pore photonic crystals. In Ref. [49], the authors demonstrate directly the fabrication of slanted pore crystals out of titanium oxide with a band gap in the visible wavelengths, using ion beam lithography. Slanted pore photonic crystals can also be fabricated using direct laser writing [50].

In this paper, we use plane wave expansion to compute the photonic band structure and electric field distributions in our proposed structure. We then compute the exciton-photon coupling strength and the critical temperature for the onset of an exciton-polariton BEC, assuming that the exciton-polaritons are non-interacting spinless bosons in a box trap. Our results suggest that thermal equilibrium above-room-temperature exciton-polariton BEC is possible with light emission near telecommunication wavelengths. By considering three 3 nm InGaAs wells surrounded by 7 nm InP barriers, we obtain a light-matter coupling strength of 13.7 meV. Using three such QWs, and by detuning the exciton 35 meV above the cavity photonic mode, we obtain a lower polariton dispersion depth of approximately 40 meV that is entirely protected within a 3D PBG. This gives a polariton effective mass of approximately 5×10^{-6} of the bare electron at the bottom of the lower polariton's dispersion. This dispersion depth also defines the energy scale for stability of the polariton with respect to thermal fluctuations. Strong-coupling implies that the polariton can form quickly compared to the time scale of thermal fluctuations. The bare exciton binding energy is only 7 meV, making it unstable to room-temperature thermal fluctuations. However, once polariton formation occurs, an energy greater than the dispersion depth must be provided by the thermal reservoir for the exciton to dissociate. This is improbable, even at room temperature. Assuming that the polaritons are trapped in a two-dimensional box trap with a side length in the range of $D = 10 - 500\,\mu$m, with an exciton density per QW of $(15a_B)^{-2}$, our calculations suggest that a thermal equilibrium BEC of polaritons could occur for temperatures as high as 436 K.

2. Polaritons in a Slanted Pore Photonic Crystal Cavity

We consider exciton-polaritons in an optical cavity composed of slanted-pore photonic crystals sandwiching a thin planar slab containing quantum wells as shown in Fig. 1(a).The central slab introduces planar guided photonic modes within the upper part of the 3D PBG [38] as shown in Fig. 1(b). We consider the strong coupling between a photon in the lowest guided photonic mode and an exciton. This results in reversible spontaneous emission and normal mode splitting into a lower and upper branch of polaritons, as shown in Fig. 1(c).

We choose the pore radius and the central slab width to have a sufficient remaining band gap between the lowest guided photonic mode and the lower bulk three-dimensional band edge to ensure that the entire lower polariton (LP) branch is protected from radiative decay. This is shown in Fig. 1(c). The periodicity in the z-direction is $\sqrt{2}a$ where a is the lattice constant (center-to-center distance between two parallel pores) of the crystal in the x-y direction so that pores criss-cross at 90 degrees. The lattice constant $a \approx 500$ nm is chosen to place the lowest guided photonic mode near resonance with the excitonic recombination energy. As the thickness of the central slab layer increases, more quantum wells can be accomodated leading to enhancement of the light-matter coupling strength. However, the remaining band gap decreases. By choosing a slab thickness of $0.07a$ and a pore radius of $0.305a$, we obtain a 3D photonic band gap with a gap-to-midgap ratio of 16% that is partially filled with 2D planar guided modes. The remaining band gap between the lowest guided photonic mode and the lower three-dimensional band edge is 10.8% and the remaining band gap between the lower

#260856 Received 17 Mar 2016; revised 13 May 2016; accepted 8 Jun 2016; published 14 Jun 2016

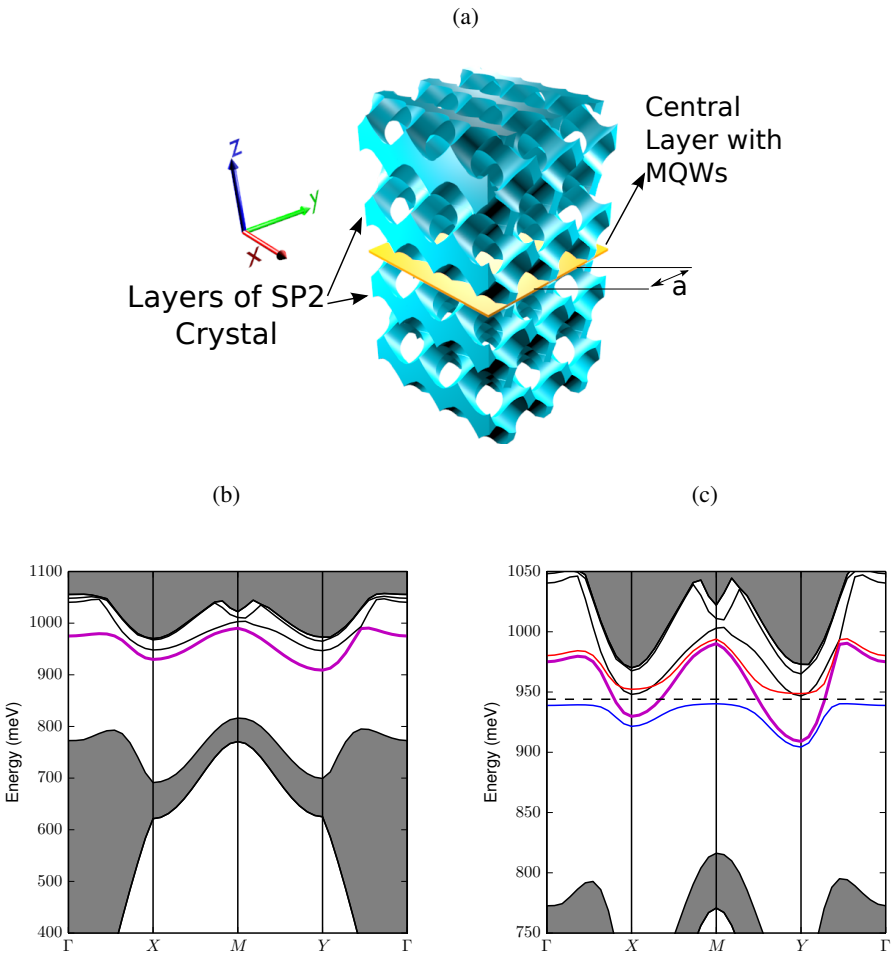

Fig. 1. (a) Slanted pore photonic crystal sandwiching a thin planar slab containing quantum wells. The pores are approximately 160 nm in radius. Three quantum wells are embedded in the central slab layer, which is approximately 36 nm in width. (b) Band structure for the heterostructure shown in Fig. 1(a) in the first Brillouin Zone of $-\pi/a \leq k_x, k_y \leq \pi/a$. The shaded grey areas represent the bulk 3D bands of the slanted pore crystal. The curves in the photonic band gap denote confined 2D guided modes introduced in the central slab layer, of which the lowest one is labelled in magenta. (c) A closer view of the band diagram around the photonic band gap. The excitonic recombination energy of $E_0 = 944$ meV (dashed black line) is detuned above the lowest guided photonic band by $\Delta = 35$ meV. The lower and upper polariton branches are shown in blue and red respectively. An exciton-photon coupling of $\hbar\Omega = 13.7$ meV is used in obtaining the polariton dispersion curves.

#260856 Received 17 Mar 2016; revised 13 May 2016; accepted 8 Jun 2016; published 14 Jun 2016

polariton dispersion minimum and the lower three-dimensional band edge is 10.2%, relative to the PBG center frequency.

The electric field of a photonic mode in the heterostructure can be written as

$$\mathbf{E}_{p,\mathbf{k}}(\rho,z)=\sqrt{\frac{\hbar\omega_{p,\mathbf{k}}}{2\varepsilon_0 S}}\mathbf{u}_{p,\mathbf{k}}(\rho,z)e^{i\mathbf{k}\cdot\rho}, \tag{1}$$

where ρ symbolizes the displacement vector in the x-y plane, z represents the vertical displacement from the center of the central slab layer in the z-direction and p is a discrete photonic band index. Since the translational symmetry of the slanted pore photonic crystal is broken only in the z-direction, each photonic mode p is further indexed by a two-dimensional wave vector $\mathbf{k}=(k_x,k_y)$ in the two-dimensional Brillouin zone of the photonic crystal such that $-\pi/a\leq k_x,k_y\leq\pi/a$. The angular frequency of a photon in the band p of wave vector $\mathbf{k}$ is $\omega_{p,\mathbf{k}}$ and ε_0 is the vacuum permittivity. S is the cross-sectional area in the x-y plane of the system and $\mathbf{u}_{p,\mathbf{k}}(\rho,z)$ is the Bloch amplitude of the electric field. To obtain the Bloch amplitudes $\mathbf{u}_{p,\mathbf{k}}(\rho,z)$, we use the MIT Photonic Bands software package [51] in which the fields are normalized so that $\frac{1}{S}\int\varepsilon(\rho,z)\left|\mathbf{u}_{p,\mathbf{k}}(\rho,z)\right|^2 d^2\rho dz=1$, where $\varepsilon(\rho,z)$ is the spatially varying dielectric function. In Fig. 2(a), we show the electric field intensity of the lowest 2D guided photonic mode over the central plane ($z=0$) of the central slab layer.

The Hamiltonian for the combined photon and exciton system in the rotating wave approximation is [52]:

$$\hat{H}=\hat{H}_{\text{exc}}+\hat{H}_{\text{ph}}+\hat{H}_{\text{int}}, \tag{2a}$$

$$\hat{H}_{\text{exc}}=\sum_{l,n,\alpha,\mathbf{k}}E_{\text{exc}}(\mathbf{k}+\mathbf{G}_n^{\parallel})\beta^{\dagger}_{l,\alpha,\mathbf{k}+\mathbf{G}_n^{\parallel}}\beta_{l,\alpha,\mathbf{k}+\mathbf{G}_n^{\parallel}}, \tag{2b}$$

$$\hat{H}_{\text{ph}}=\sum_{p,\mathbf{k}}\hbar\omega_{p,\mathbf{k}}\hat{a}^{\dagger}_{p,\mathbf{k}}\hat{a}_{p,\mathbf{k}}, \tag{2c}$$

$$\hat{H}_{\text{int}}=\sum_{l,\alpha,n,p,\mathbf{k}}i\hbar\tilde{\Omega}_{l,\alpha,n,p,\mathbf{k}}\beta^{\dagger}_{l,\alpha,\mathbf{k}+\mathbf{G}_n^{\parallel}}a_{p,\mathbf{k}}+h.c., \tag{2d}$$

where $\hat{H}_{\text{exc}}$, $\hat{H}_{\text{ph}}$ and $\hat{H}_{\text{int}}$ are the excitonic, photonic and interaction terms of the Hamiltonian, respectively. $E_{\text{exc}}(\mathbf{k})$ is the energy of an exciton with center-of-mass wave vector $\mathbf{k}$ and $\mathbf{G}_n^{\parallel}=(n_x,n_y)\frac{2\pi}{a}$ is a reciprocal lattice vector for the 3D photonic crystal parallel to the QW plane. $\beta_{l,\alpha,\mathbf{k}}$ is the annihilation operator for an exciton [53, 54] in the l^{th} quantum well, with wave vector $\mathbf{k}$ and polarization α. The polarization α can be either longitudinal (L), transverse (T) or normal (Z). For L and T excitons, the exciton's polarization vector is in the plane of the quantum well and is, respectively, parallel or perpendicular to the exciton's center of mass wave vector that also lies in the plane of the quantum well. For Z excitons, the exciton's polarization vector is normal to the quantum well plane, regardless of the exciton's center of mass wave vector. In this work, we focus on the L and T polarizations of the exciton, since in the central slab layer the z-component of the electric field of the lowest guided mode is much weaker than the x- and y-components, as shown in Fig. 2(b). As a result, the coupling of the electric field to the Z-excitons will be weaker than for the L and T polarizations. In Eq. (2c), $\hat{a}_{p,\mathbf{k}}$ is the annihilation operator of a photon of frequency $\omega_{p,\mathbf{k}}$ in the p^{th} band with wave vector $\mathbf{k}$. In the interaction term, $\tilde{\Omega}_{l,\alpha,n,p,\mathbf{k}}$ represents the coupling strength between an exciton of polarization α and wave vector $\mathbf{k}+\mathbf{G}_n^{\parallel}$ in the l^{th} quantum well with a photon in the p^{th} band of wave vector $\mathbf{k}$. The coupling strength is given by [52]

$$\tilde{\Omega}_{l,\alpha,n,p,\mathbf{k}}=\frac{E_{\text{exc}}(\mathbf{k}+\mathbf{G}_{\parallel}^{n})}{\hbar\sqrt{2\hbar\omega_{p,\mathbf{k}}\varepsilon_0}}\phi(0)d_{\alpha}\left(\mathbf{u}_{p,\mathbf{k}+\mathbf{G}_{\parallel}^{n}}(\rho,z_l)\cdot\hat{\mathbf{n}}_{\alpha}\right), \tag{3}$$

#260856 Received 17 Mar 2016; revised 13 May 2016; accepted 8 Jun 2016; published 14 Jun 2016

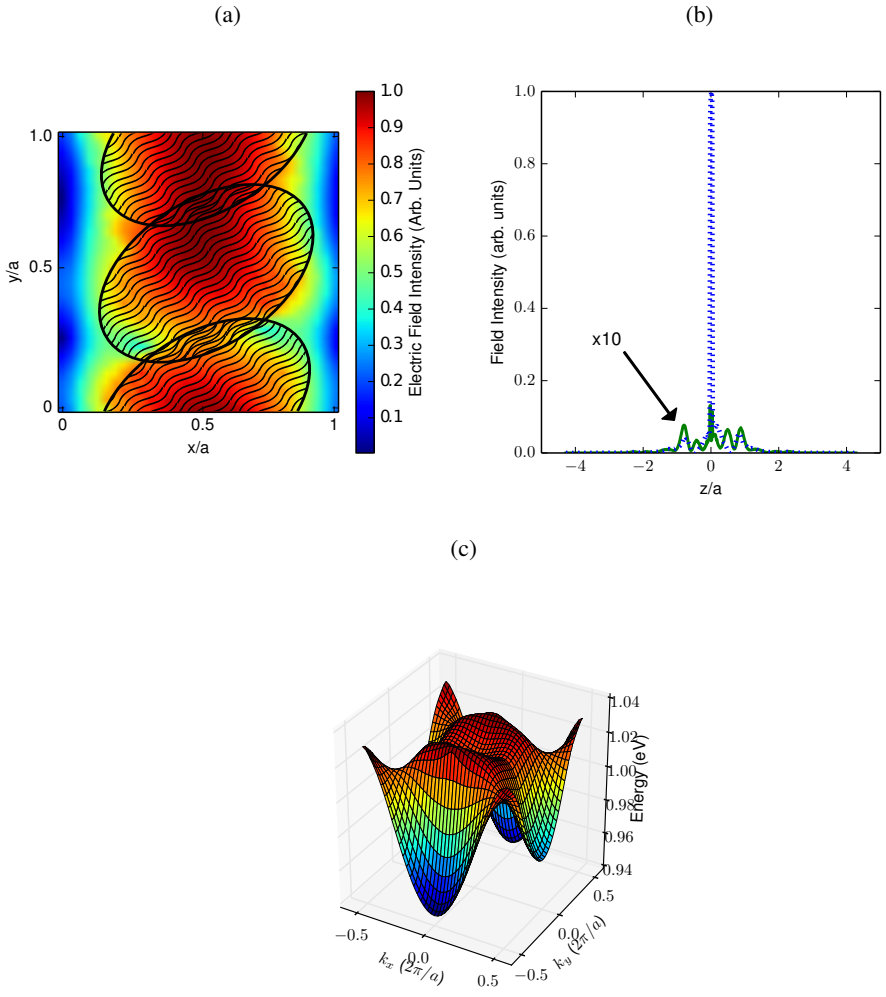

Fig. 2. (a) Electric field intensity in the QW region for the lowest guided mode over the area occupied by one unit cell of slanted pore photonic crystal. The slice is in the x-y plane at a height of $z = 0$, through the middle of the central slab layer. The patterned areas indicate the regions where the air pores make contact with the central slab layer. (b) Average in-plane field intensity for the lowest guided photonic mode at wave vector $\mathbf{Q}^{(Y)} = (0, 0.5)\frac{2\pi}{a}$ (dotted line) $\frac{1}{S}\int_S \sum_{\alpha=L,T}(\mathbf{u}_{\mathbf{Q}^{(Y)}}(\rho,z)\cdot\hat{\mathbf{n}}_\alpha)^2 d^2\rho$, and that of the z-component (solid line, multiplied by a factor of 10) $\frac{1}{S}\int_S(\mathbf{u}_{\mathbf{Q}^{(Y)}}(\rho,z)\cdot\hat{\mathbf{n}}_Z)^2 d^2\rho$ as a function of the vertical position z in the heterostructure. (c) Photonic dispersion $\hbar\omega_{\mathbf{k}}$ for the lowest guided photonic mode over the first photonic Brillouin Zone. The lattice constant $a = 495$ nm is chosen so that the exciton is resonant with the lowest guided photonic mode.

#260856 Received 17 Mar 2016; revised 13 May 2016; accepted 8 Jun 2016; published 14 Jun 2016

where $\phi(0)$ represents the amplitude of the excitonic wave function at zero electron-hole separation [52–54] and d_α is the dipole transition matrix element of an exciton with polarization $\alpha = L,T$. $\mathbf{u}_{p,\mathbf{k}+\mathbf{G}_n^\parallel}$ is the Bloch amplitude of the electric field from Eq. (1), z_l is the height from the center of the central slab layer at which the l^{th} quantum well is situated and $\hat{\mathbf{n}}_\alpha$ is a unit vector that points along the longitudinal ($\alpha = L$) or transverse ($\alpha = T$) direction.

The excitonic dispersion in Eq. (2b) can be written under the effective mass approxmation [1] as

$$E_{\text{exc}}(\mathbf{k}) = E_0 + \frac{\hbar^2}{2m_{\text{exc}}}k^2, \tag{4}$$

where E_0 = 944 meV is the recombination energy for excitons in 3 nm InGaAs quantum wells with 7 nm InP barriers at zero center-of-mass wave vector and $m_{\text{exc}} = 0.11\,m_0$ [55] where $m_0 = 9.11\times10^{-31}$ kg is the bare electron mass. Figure 2(c) depicts the photonic dispersion $\hbar\omega_{\mathbf{k}}$ of the lowest guided band in the photonic Brillouin zone. In the vicinity of the local minimum $\mathbf{Q}^{(Y)} = (0,0.5)\frac{2\pi}{a}$ (the Y-point of the band diagrams in Figs. 1(b) and 1(c), the photonic dispersion in the effective mass approximation becomes

$$\hbar\omega_{\mathbf{k}} = \hbar\omega_0 + \frac{\hbar^2}{2}\left(\frac{(k_x - Q_x^{(Y)})^2}{m_x^{(Y)}} + \frac{(k_y - Q_y^{(Y)})^2}{m_y^{(Y)}}\right). \tag{5}$$

With an appropriate choice of the lattice constant a, the energy minimum of the lowest guided photonic mode $\hbar\omega_0$ can be made close to the exciton recombination energy of E_0. Taking the lattice constant to be $a = 516$ nm, we find that $\hbar\omega_0$ = 909 meV (35 meV below the exciton recombination energy) and the effective mass along the x-direction at the Y-point is $m_x^{(Y)} = 3.08\times10^{-6}\,m_0$ and along the y-direction is $m_y^{(Y)} = 9.11\times10^{-6}\,m_0$.

In the sum over p in Eq. (2), we retain only the lowest guided photonic band. In this case, the effective exciton-photon Hamiltonian becomes:

$$\hat{H} = \hat{H}_0 + \hat{H}_{\text{int}}, \tag{6a}$$

$$\hat{H}_0 = \sum_{\mathbf{k}}\left[E_{\text{exc}}(\mathbf{k})\hat{b}_{\mathbf{k}}^\dagger\hat{b}_{\mathbf{k}} + \hbar\omega_{\mathbf{k}}\hat{a}_{\mathbf{k}}^\dagger\hat{a}_{\mathbf{k}}\right], \tag{6b}$$

$$\hat{H}_{\text{int}} = \sum_{\mathbf{k}} i\hbar\Omega_{\mathbf{k}}\left(\hat{b}_{\mathbf{k}}^\dagger\hat{a}_{\mathbf{k}} - \hat{b}_{\mathbf{k}}\hat{a}_{\mathbf{k}}^\dagger\right), \tag{6c}$$

where we have defined a collective exciton operator $\hat{b}_{\mathbf{k}}$ such that

$$\hat{b}_{\mathbf{k}} = \sum_{l,\alpha,n}\frac{\tilde{\Omega}_{l,\alpha,n,\mathbf{k}}}{\Omega_{\mathbf{k}}}\beta_{l,\alpha,\mathbf{k}+\mathbf{G}_n^\parallel}, \tag{7a}$$

$$\Omega_{\mathbf{k}} = \sqrt{\sum_{l,n,\alpha}\tilde{\Omega}^*_{l,\alpha,n,\mathbf{k}}\tilde{\Omega}_{l,\alpha,n,\mathbf{k}}}. \tag{7b}$$

$\hat{b}_{\mathbf{k}}$ annihilates an excitation of energy $E_{\text{exc}}(\mathbf{k})$ that is a superposition of excitons in quantum wells indexed by l, polarizations indexed by $\alpha = L,T$, and momenta indexed by $\mathbf{k}+\mathbf{G}_\parallel^n$, weighted by the factor $\frac{\tilde{\Omega}_{l,\alpha,n,\mathbf{k}}}{\Omega_{\mathbf{k}}}$. The collective coupling constant $\Omega_{\mathbf{k}}$ represents the coupling strength of an excitation created by $\hat{b}_{\mathbf{k}}^\dagger$ to photons that have a wave vector $\mathbf{k}$.

To obtain the collective coupling strength $\Omega_{\mathbf{k}}$, we compute the sum in Eq. (7b), using Eq. (3). We assume that the dipole transition matrix elements in the longitudinal and transverse directions are approximately equal, and we write $d_\alpha \approx d$ for $\alpha = L,T$ to find that

#260856 Received 17 Mar 2016; revised 13 May 2016; accepted 8 Jun 2016; published 14 Jun 2016

$\Omega_{\mathbf{k}}^2 = E_{\text{exc}}(\mathbf{k})^2/(2\hbar^3\omega_{\mathbf{k}}\varepsilon_0)\,|\phi(0)|^2\,|d|^2\sum_{l,n}\left|\mathbf{u}_{\mathbf{k}+\mathbf{G}_\parallel^n}(\rho,z_l)\right|^2$. We then apply Parseval's theorem, which states that if a function can be written as a Fourier series over a region $A=[-L/2,L/2]\times[-L/2,L/2]$ as $f(\rho)=\sum_n f_n\exp(i\mathbf{q}_n\cdot\rho)$ where $\mathbf{q}_n=\frac{2\pi}{L}(n_x,n_y)$ with n_x,n_y being integers, then $\sum_n|f_n|^2=\frac{1}{L^2}\int_A|f(\rho)|^2\,d^2\rho$ [56]. Applying Parseval's theorem to the Bloch amplitudes $\mathbf{u}_{\mathbf{k}+\mathbf{G}_\parallel^n}(\rho,z_l)$, the collective coupling strength becomes:

$$\Omega_{\mathbf{k}}=\frac{E_0}{\hbar\sqrt{2\hbar\omega_{\mathbf{k}}\varepsilon_0 S}}\,|\phi(0)|\,|d|\left[\sum_l\int_S|\mathbf{u}_{\mathbf{k}}(\rho,z_l)|^2\,d^2\rho\right]^{1/2}. \tag{8}$$

Diagonalizing the Hamiltonian in Eq. (6) yields the dispersion relation of the lower polariton branch

$$E_{\text{LP}}(\mathbf{k})=\frac{1}{2}\left(E_{\text{exc}}(\mathbf{k})+\hbar\omega_{\mathbf{k}}-\sqrt{(E_{\text{exc}}(\mathbf{k})-\hbar\omega_{\mathbf{k}})^2+4\hbar^2\Omega^2}\right), \tag{9}$$

where we have replaced $\Omega_{\mathbf{k}}$ with its value, Ω, at $\mathbf{k}=\mathbf{Q}^{(Y)}$. This is possible because $\Omega_{\mathbf{k}}$ varies very little in the immediate vicinity of $\mathbf{Q}^{(Y)}$ where the LP minimum occurs, as shown in Fig. 3(a). In Fig. 3(b), we show the lower polariton's dispersion over the first photonic Brillouin zone where we assume an exciton with a recombination energy of $E_0=944$ meV is resonant with the lowest guided photonic mode at $\mathbf{Q}^{(Y)}$. The resulting collective coupling strength is $\hbar\Omega=13.7$ meV using three quantum wells in the central slab layer.

We define the dispersion depth V of the LP branch as the difference in energy between the exciton and the LP branch at $\mathbf{Q}^{(Y)}$:

$$\begin{aligned}V&=[E_{\text{exc}}(\mathbf{k})-E_{\text{LP}}(\mathbf{k})]_{\mathbf{k}=\mathbf{Q}^{(Y)}}\\&=\Delta/2+\sqrt{(\Delta/2)^2+\hbar^2\Omega^2},\end{aligned} \tag{10}$$

where $\Delta=[E_{\text{exc}}(\mathbf{k})-\hbar\omega_{\mathbf{k}}]_{\mathbf{k}=\mathbf{Q}^{(Y)}}=E_0-\hbar\omega_0$ is the exciton-photon detuning. Here we neglect the excitonic dispersion, since the exciton is five orders of magnitude heavier than the cavity photon. We illustrate both V and Δ in Fig. 3(c). The dispersion depth plays a crucial role in determining the critical temperature T_c for the onset of an exciton-polariton BEC. In particular, $k_BT_c\lesssim V$ [45]. For temperatures small compared to V/k_B, polaritons occupy mainly the low-energy photonlike states near the minimum of the LP branch with a reduced effective mass. Conversely, for temperatures on the order of or larger than V/k_B, the polaritons occupy higher energy excitonlike states for which the effective mass is nearly that of the excitons themselves. In the latter case, the polariton density required for the onset of the BEC is very large. However, such polariton densities are usually unattainable, since the density of the polaritons' excitonic component is bounded above by the saturation density [57], at which exciton-exciton collisions cause the excitons to dissociate. Therefore, we do not expect a polariton BEC for temperatures greater than V/k_B, no matter how small the effective mass near the minimum of the LP branch.

3. Photonic Structure Optimization

In this section, we examine the conditions necessary for obtaining a thermal equilibrium room-temperature BEC of exciton-polaritons. In particular, we examine how the dispersion depth can be optimized with realistic choices of coupling strength $\hbar\Omega$ and detuning Δ. We also examine limitations on detuning for the thermalization of the exciton-polaritons.

Using more than one quantum well will increase the light-matter coupling between excitons and photons up to a factor of $\sqrt{N_{QW}}$ where N_{QW} is the number of quantum wells in the system. The maximum enhancement occurs if the electric field intensity is the same in all

#260856 Received 17 Mar 2016; revised 13 May 2016; accepted 8 Jun 2016; published 14 Jun 2016

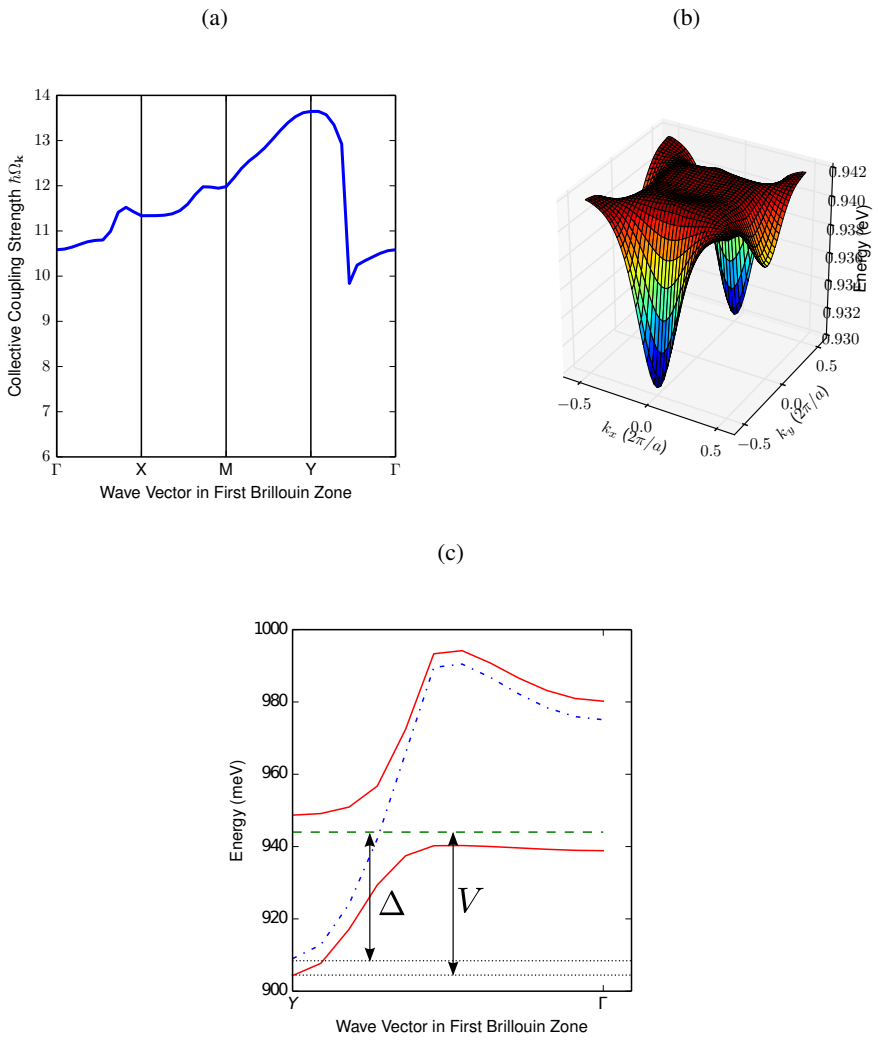

Fig. 3. (a) The collective coupling strength $\hbar\Omega_{\mathbf{k}}$ over the high symmetry path in the first photonic Brillouin Zone. We compute $\hbar\Omega_{\mathbf{k}}$ assuming there are three QWs in the central slab layer and a detuning of $\Delta = 35$ meV. (b) The dispersion of the lower polariton branch from Eq. (9). The collective coupling strength is $\hbar\Omega = 13.7$ meV for three QWs placed in the central slab layer. The lattice constant is $a = 495$ nm to enforce a detuning of $\Delta = 0$. In both Figs. (a) and (b), the QWs are composed of 3 nm InGaAs wells surrounded by 7 nm InP barriers and the central slab layer is $0.07a$ thick. (c) The dispersion depth V and the detuning Δ. The excitonic dispersion (dashed green), lowest guided 2D photonic band dispersion (dash-dot blue) and the lower and upper polariton dispersions (solid red) are shown from the local photonic minimum at $\mathbf{k} = \mathbf{Q}^{(Y)}$ to $\mathbf{k} = 0$.

#260856 Received 17 Mar 2016; revised 13 May 2016; accepted 8 Jun 2016; published 14 Jun 2016

quantum wells. This follows from the symmetrization and normalization of the exciton wave function. Let the state vector of an exciton of in the j^{th} quantum well be $\left|\phi_j\right\rangle$. Assuming that the field amplitude is the same in all quantum wells, there is an equal probability that the exciton can be excited in any of the N_{QW} quantum wells. Therefore, the state vector for the exciton in the multiple-quantum well system can be written as $|\Psi\rangle = \frac{1}{\sqrt{N_{QW}}}\sum_{j=1}^{N_{QW}}\left|\phi_j\right\rangle$. The coupling strength for multiple quantum wells is defined as the transition amplitude $\hbar\Omega_{MQW} = \left\langle \Psi, 0^{\text{photon}}\right| \hat{H}_I \left|0, 1^{\text{photon}}\right\rangle$ where $\hat{H}_I = \sum_{j=1}^{N_{QW}} \hat{H}_I^j$ is the exciton-photon interaction Hamiltonian for the multiple quantum well system and $\hat{H}_I^j$ is the exciton-photon Hamiltonian for the j^{th} quantum well alone. The coupling strength for a single quantum well is given by $\hbar\Omega_{QW} = \left\langle \phi_j, 0^{\text{photon}}\right| \hat{H}_I \left|0, 1^{\text{photon}}\right\rangle$ which is independent of j, based on the assumption that the field amplitude is the same in each of the quantum wells. It then follows that $\Omega_{MQW}/\Omega_{QW} = N_{QW}/\sqrt{N_{QW}} = \sqrt{N_{QW}}$. This increase in the collective coupling strength by considering N_{QW} quantum wells is analagous to the Dicke model in atomic systems, where the collective light-matter coupling strength of an assembly of N two-level atoms increases by a factor of $\sqrt{N}$ relative to a single two level atom [54]. Another advantage to using multiple quantum wells is that the exciton density in any single quantum well can be considerably below the saturation density.

We consider the structure shown in Fig. 1(a), in which a $0.07a$ central slab layer is sandwiched by periods of double slanted pore (SP2) crystals with a pore radius of $0.305a$. The lattice constant a is chosen to be 516 nm to realize a detuning of $\Delta = 35$ meV. We consider all quantum wells to be composed of 3 nm InGaAs wells surrounded by 7 nm InP barriers. To obtain the largest possible enhancement to the coupling strength, we consider both the cases of QWs only in the central slab layer and the case of additional QWs in the first unit cell of SP2 both above and below the central slab layer. We start by placing a single QW in the central slab layer, for which we obtain $\hbar\Omega = 8.0$ meV. We increment the number of QWs in the central slab layer until we reach the maximum capacity of three QWs in the central slab to obtain $\hbar\Omega = 13.7$ meV. By maximally occupying the central slab layer with three QWs, there is a nearly $\sqrt{3}$ enhancement of $\hbar\Omega$ relative to one QW because the average field intensity of the field $\mathbf{u}_{\mathbf{Q}^{(Y)}}(\rho, z)$ over the x-y plane is the same in each quantum well. We then place the fourth QW in the SP2 crystal above the central slab layer and we place the fifth QW in the SP2 crystal below. We continue to symmetrically add QWs above and below the central slab layer until the first unit cell of SP2 both above and below the central slab layer is saturated with 149 QWs. This yields a collective coupling strength of $\hbar\Omega$=20.2 meV. The results of this calculation are shown in Fig. 4. The increase in $\hbar\Omega$ in the vicinity of $N_{\text{QW}} = 70$ can be understood by examining the average field intensity of the lowest guided mode $\mathbf{u}_{\mathbf{Q}^{(Y)}}(\rho, z)$ over the x-y plane as a function of vertical height z (see Fig. 2(b)). The increase in $\hbar\Omega$ (see Eq. (7b)) in the vicinity of $N_{\text{QW}} = 70$ occurs because there is a small secondary peak in the field intensity at $z \approx \pm 0.75a \approx \pm 400$ nm, which are the z-positions of the 70^{th} and nearby QWs.

Our maximum coupling occurs when the central slab layer and the first unit cell of SP2 both above and below the central slab layer are saturated with a total of 149 QWs ($\hbar\Omega = 20.2$ meV). We expect quantum coherence can be maintained across all QWs placed within a range of $(2\sqrt{2}+0.07)a = 1496$ nm which is on the order of one optical wavelength corresponding to exciton recombination at $\frac{hc}{E_0} = 1313$ nm.

While pores in the QWs outside the central slab layer cause surface recombination of excitons, this effect can be mitigated by coating the inner surface of the pores with an approximately 10 nm wide layer of InP. Such a coating does not significantly alter the band structure of the heterostructure from that shown in Fig. 1(b), and a 10.1% PBG between the LP dispersion minimum and the lower three-dimensional band edge remains. However, fabrication of a

#260856 Received 17 Mar 2016; revised 13 May 2016; accepted 8 Jun 2016; published 14 Jun 2016

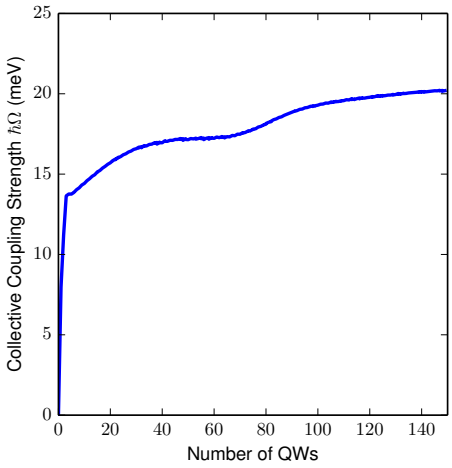

Fig. 4. The collective coupling strength $\hbar\Omega$ as a function of the number of (3 nm thick) InGaAs QWs (with 7 nm InP barriers) embedded in the heterostructure. The lattice constant $a = 516$ nm provides an exciton-photon detuning of $\Delta = 35$ meV. The first three QWs are placed in the central slab layer, and subsequent QWs are placed in the photonic crystal above and below the central slab layer.

heterostructure containing 149 QWs is challenging. The more easily accessible structure with only three QWs in the central slab layer enables a sufficiently large LP dispersion depth ($V = 40$ meV) to realize room temperature equilibrium BEC.

We also consider the effect of varying the quantum well width on the collective coupling strength $\hbar\Omega$. Specifically, we consider varying the width of the InGaAs QWs from 2 nm to 5 nm, while holding the InP barrier width fixed at 7 nm. As the quantum well width increases, the exciton binding energy decreases. The exciton binding energy and the recombination energy as a function of QW width are depicted in Fig. 5(a). These are calculated, following the computational procedure outlined in [58], taking the conduction electron and valence hole to have masses of $m_e = 0.01m_0$ [55] and $m_h = 0.10m_0$ [59], respectively. We then compute the coupling strength $\hbar\Omega$ using a $0.07a$ central slab layer, sandwiched by SP2 crystals. The lattice constant a varies between 475 nm and 570 nm to enforce a detuning of $\Delta = 35$ meV, as shown in Fig. 5(b). Figure 5(c), depicts the coupling strength $\hbar\Omega$ for various choices of the QW width in the central slab layer (three QWs), and for QWs filling the central slab and the first unit cell of SP2 above and below the central slab (approximately 150 QWs). Based on these results, the optimal QW width is 3 nm. This choice facilitates an exciton recombination energy ($E_0 = 944$ meV) close to the telecommunications band with a large collective coupling strength within the central slab layer, using three QWs.

Although a large detuning Δ provides a large dispersion depth, it causes longer thermalization times for the exction-polaritons. For $\Delta > 0$, the LP branch is more photonlike, and polariton-phonon scattering is the dominant thermalization mechanism, while for $\Delta < 0$, the LP branch is more excitonlike and polariton-polariton scattering is more dominant [9]. While polariton-polariton scattering can thermalize the polariton gas, it cannot reduce the energy of the gas. Polariton-phonon scattering provides the dissipative cooling mechanism for the polaritons. We choose $\Delta > 0$ to increase the dispersion depth V, by a judicious choice of the lattice

#260856 Received 17 Mar 2016; revised 13 May 2016; accepted 8 Jun 2016; published 14 Jun 2016

constant a, as shown in Fig. 5(d). For $\Delta = 35$ meV, ($a = 516$ nm), and with a $0.07a$ central slab layer containing three QWs ($\hbar\Omega = 13.7$ meV), the dispersion depth is $V = 40$ meV. This provides a generous upper bound of 460 K on the critical temperature for the onset of an exciton-polariton BEC. In 3 nm InGaAs QWs with 7 nm InP barriers, the exciton-LO phonon scattering time at room temperature is approximately 0.5 ps [60–62]. At a detuning of $\Delta = 35$ meV, the exciton-polaritons have an exciton fraction per QW of approximately 3% which suggests a room temperature polariton-phonon scattering time of approximately 16 ps. We also estimate the exciton-exciton scattering time, based on theory [63, 64] and experiment [65] in InGaAs quantum wells with InP barriers to be approximately 1 ps. Therefore, at a detuning of $\Delta = 35$ meV, where the exciton-polaritons have an exciton fraction per QW of approximately 3%, we estimate that polariton-polariton scattering time is approximately 30 ps. The radiative decay of the exciton-polaritons is strongly inhibited by the 3D PBG of the SP2 crystals. Experimental study of optical cavities with photonic crystals [39, 66] suggests that the photonic lifetime in such cavities may range from 500 ps to 1 ns. Due to this extremely strong suppression of radiative decay, the exciton-polaritons decay non-radiatively on a time scale of about 200 ps at room temperature [40]. This is sufficient time for the exciton-polaritons to reach self-equilibrium and thermalize with their host lattice for full thermal equilibrium.

4. Exciton-Polariton BEC

It is well known that the formation of a BEC of identical non-interacting bosons in an infinite two-dimensional system is forbidden by the Mermin-Wagner theorem [67, 68]. However, in a finite two-dimensional system, a phase transition at a finite temperature T_c is possible due to the discretization of the particles' energy spectrum [69, 70]. Accordingly, we consider exciton-polaritons confined in a finite two-dimensional box trap, in which the central slab layer has a finite length D in the x- and y-directions. Such finite-sized two-dimensional slab defects have been fabricated by Ogawa *et. al.* [71, 72]. Their structure consists of woodpile photonic crystals sandwiching a 0.5 μm to 3 μm sized InGaAsP multiple QW layer to emit light in the range of 1.45 μm to 1.60 μm, around the telecommunications wavelength of 1.5 μm.

To compute the critical temperature T_c for the onset of an exciton-polariton BEC, we assume that the excitons are confined using a box trap with infinitely high potential barriers for $|x|, |y| \geq D/2$. The two-dimensional confinement induces a discrete spectrum $E_{\mathrm{LP}}(\mathbf{k}_{n_x,n_y})$ for the exciton-polaritons' energy where $\mathbf{k}_{n_x,n_y} = \mathbf{Q}^{(Y)} + (n_x, n_y)\frac{\pi}{D}$ are the discrete momentum states around $\mathbf{Q}^{(Y)}$ for positive integers n_x and n_y. The critical temperature T_c is computed using the Ketterle-van Druten criterion as [73]

$$\sum_{n_x,n_y>1}^{\infty} \frac{1}{\exp\left(E_{\mathrm{LP}}(\mathbf{k}_{n_x,n_y})/k_B T_c\right) - 1} = N, \tag{11}$$

where k_B is the Boltzmann constant, $N = \rho_{\mathrm{pol}}^{\mathrm{tot}} D^2$ is the total number of exciton-polaritons in the box trap and $\rho_{\mathrm{pol}}^{\mathrm{tot}}$ is the total polariton density. The Ketterle-van Druten criterion associates T_c for BEC (for fixed trapping area and polariton density) as a crossover temperature to macroscopic occupation of the ground state when the combined occupancy of the excited states equals the total number of polaritons in the trapping area. The ground state at $\mathbf{k}_{1,1}$ in which the BEC forms is explicitly excluded from the sum in (11). An alternate criterion for T_c is the Onsager criterion, which defines the crossover to a BEC when $N_0/N = 0.1$ where N_0 is the number of particles in the ground state. This criterion provides a slightly lower estimate for the critical temperature T_c than the Ketterle-van Druten criterion [45, 74].

When choosing the polariton density ρ_{pol}, we take into account that the exciton-polariton is a superposition of an exciton and a photon and that the excitonic component is distributed

#260856 Received 17 Mar 2016; revised 13 May 2016; accepted 8 Jun 2016; published 14 Jun 2016

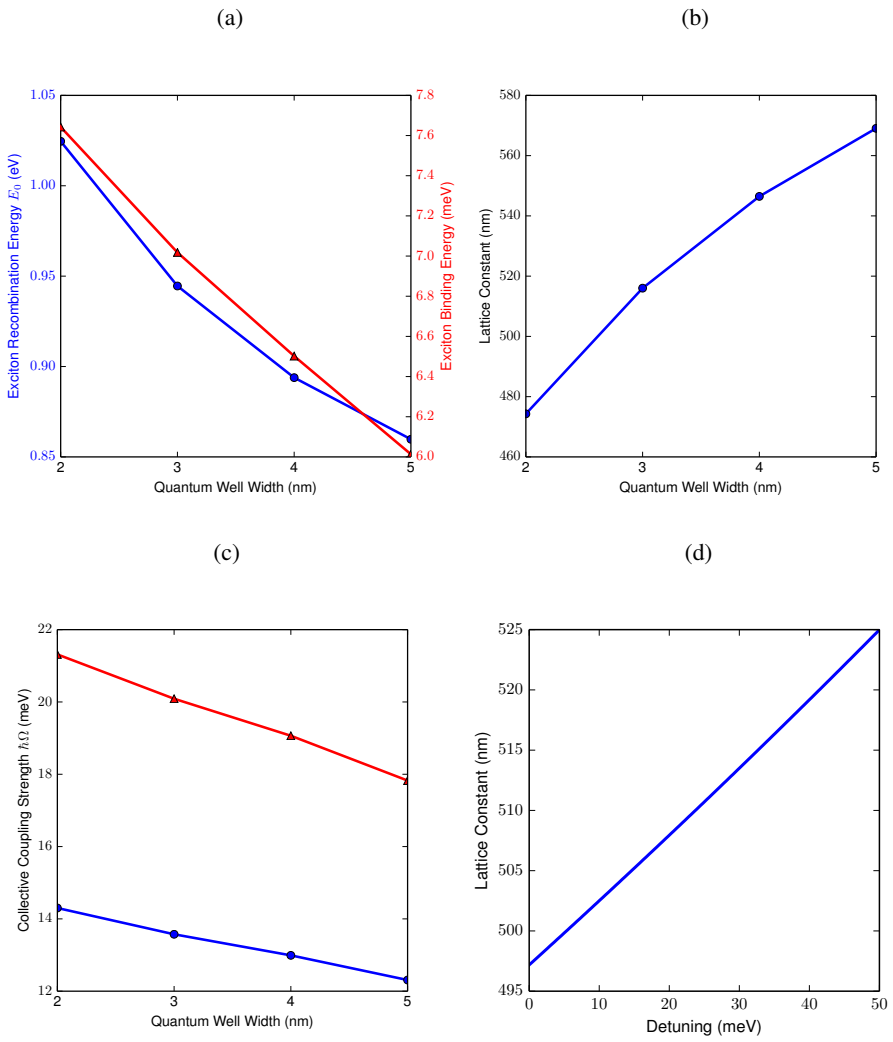

Fig. 5. (a) The exciton recombination energy E_0 (circles) and the exciton binding energy (triangles) in InGaAs quantum wells of varying widths surrounded by 7 nm InP barriers. (c) The lattice constant a (circles) required to enforce a detuning of $\Delta = 35$ meV for each QW width. For each QW width, the central slab layer accomodates three QWs. (c) The collective coupling strength versus the QW width, assuming there are only QWs in the central slab layer (circles) and that the first unit cell of SP2 above and below the central slab layer are saturated with QWs (triangles). (d) The relationship between detuning Δ and the lattice constant a for a $0.07a$ central slab layer sandwiched by SP2 photonic crystal with a pore radius of $0.305a$. The exciton recombination energy is 944 meV, which is that for 3 nm InGaAs QWs surrounded by 7 nm InP barriers.

#260856 Received 17 Mar 2016; revised 13 May 2016; accepted 8 Jun 2016; published 14 Jun 2016

over multiple QWs. In particular, we must ensure that the average excitonic density in each QW remains below the saturation density, at which exciton-exciton collisions cause dissociation [2]. The excitonic density may not be the same in each QW because the exciton fraction, determined by $\tilde{\Omega}_{l,\alpha,n,p,\mathbf{k}}$, varies between the different QWs. According to Ref. [57], the exciton saturation density is $(5a_B)^{-2}$, where a_B is the excitonic Bohr radius. In 3 nm InGaAs QWs with 7 nm InP barriers, the exciton Bohr radius is 10 nm, yielding an excitonic saturation density of $400\,\mu\mathrm{m}^{-2}$ in one QW. To avoid excitonic dissociation, we choose polariton densities such that the effective exciton density in each QW remains below $\rho_{\mathrm{exc}}^{\mathrm{max}} = (15a_B)^{-2} = 44\,\mu\mathrm{m}^{-2}$.

By considering three QWs in the central slab layer and a detuning of $\Delta = 35$ meV, the exciton fraction in each of the QWs is $|X_l|^2 \equiv \frac{1}{2}\left(1 - \frac{\Delta}{\sqrt{\Delta^2+4\hbar^2\Omega^2}}\right)\frac{\Omega_l^2}{\Omega^2} = 3.6\%$, where $\Omega_l^2 = \frac{E_0^2}{2\hbar^3\omega_{\mathbf{Q}^{(Y)}}\varepsilon_0 S}|\phi(0)|\,|d|^2\int_S \left|\mathbf{u}_{\mathbf{Q}^{(Y)}}(\boldsymbol{\rho},z_l)\right|^2 d^2\boldsymbol{\rho}$ (see Eqs. (3), (7b) and (8)). The collective coupling strength is $\Omega^2 = \sum_l \Omega_l^2$ and the total exciton fraction of the polaritons is $|X|^2 = \sum_l |X_l|^2$. In our case, $f_{\mathrm{max}} = \max\{|X_l|^2\} = 3.6\%$. Subsequently, we choose a maximum polariton density per QW of $\rho_{\mathrm{pol}}^{\mathrm{max}} = \rho_{\mathrm{exc}}^{\mathrm{max}}/f_{\mathrm{max}}$, which in our case amounts to $\rho_{\mathrm{pol}}^{\mathrm{max}} = (2.8a_B)^{-2} = 1.2\times10^3\ \mu\mathrm{m}^{-2}$.

In Fig. 6, we present numerical results of T_c for various cavity lengths, detunings and number of QWs at a fixed polariton density per QW of $\rho_{\mathrm{pol}} = (6.2a_B)^{-2} = 260\,\mu\mathrm{m}^{-2}$. This polariton density per QW is chosen so as to ensure at zero detuning ($f_{\mathrm{max}} = 17\%$) that the exciton density in each QW remains below $(15a_B)^{-2}$. Our results suggest that a room-temperature exciton-polariton BEC is possible for a range of cavity lengths and for as few as three QWs. The dependence of T_c on the cavity length D in Fig. 6(a) is consistent with the Mermin-Wagner theorem. T_c tends slowly toward zero for increasingly large cavity sizes. However, T_c decreases substantially only for cavity lengths greater than $D \approx 1$ cm. Our results suggest that room-temperature BEC is possible for cavity lengths $10\,\mu\mathrm{m} \le D \le 10^3\,\mu\mathrm{m}$ and for a modest polariton density per QW of $(6.2a_B)^{-2}$. Figure 6(b) shows that the critical temperature increases with coupling strength and detuning, consistent with expected rise of T_c with dispersion depth V. In Fig. 6(c), we observe that the greatest gains in T_c occur by adding the first three QWs into the central slab layer. Although additional QWs in the cladding further elevate T_c, they are not nearly as effective.

In Fig. 7, we depict the effect of polariton density on the critical temperature T_c. In Figs. 7(a), 7(b) and 7(c), the maximum polariton density per QW is chosen to be $(2.8a_B)^{-2} = 1.2\times10^3\,\mu\mathrm{m}^{-2}$. The critical temperature is clearly most sensitive to the density. As the interparticle spacing between the polaritons $\rho_{\mathrm{pol}}^{-1/2}$ decreases, the temperature at which the de Broglie wavelength exceeds $\rho_{\mathrm{pol}}^{-1/2}$ increases. Figure 7(c) verifies that the critical temperature is also very sensitive to the detuning Δ and that it is limited by the dispersion depth V. Together, our results in Figs. 6 and 7 suggest that with a cavity length of $D = 50\,\mu\mathrm{m}^{-2}$, a detuning of $\Delta = 35$ meV and with only three QWs in the central slab layer, room-temperature equilibrium BEC of exciton-polaritons is possible.

5. Effects of Structural Disorder

We now examine the effects of structural disorder on the critical temperature for exciton-polariton BEC. Such disorder may arise in the photonic crystal cladding and in the QW active layers during fabrication. We refer to these as photonic and electronic disorder, respectively.

We model photonic disorder by varying the pore radius r_p between $0.296a$ and $0.314a$ throughout the entire photonic crystal cladding, representing a $\pm3\%$ variation about the optimal $0.305a$. We hold the lattice constant fixed at 516 nm, to enforce a detuning of $\Delta = 35$ meV for a $0.07a$ central slab layer surrounded by slanted pore photonic crystal with an ideal

#260856 Received 17 Mar 2016; revised 13 May 2016; accepted 8 Jun 2016; published 14 Jun 2016

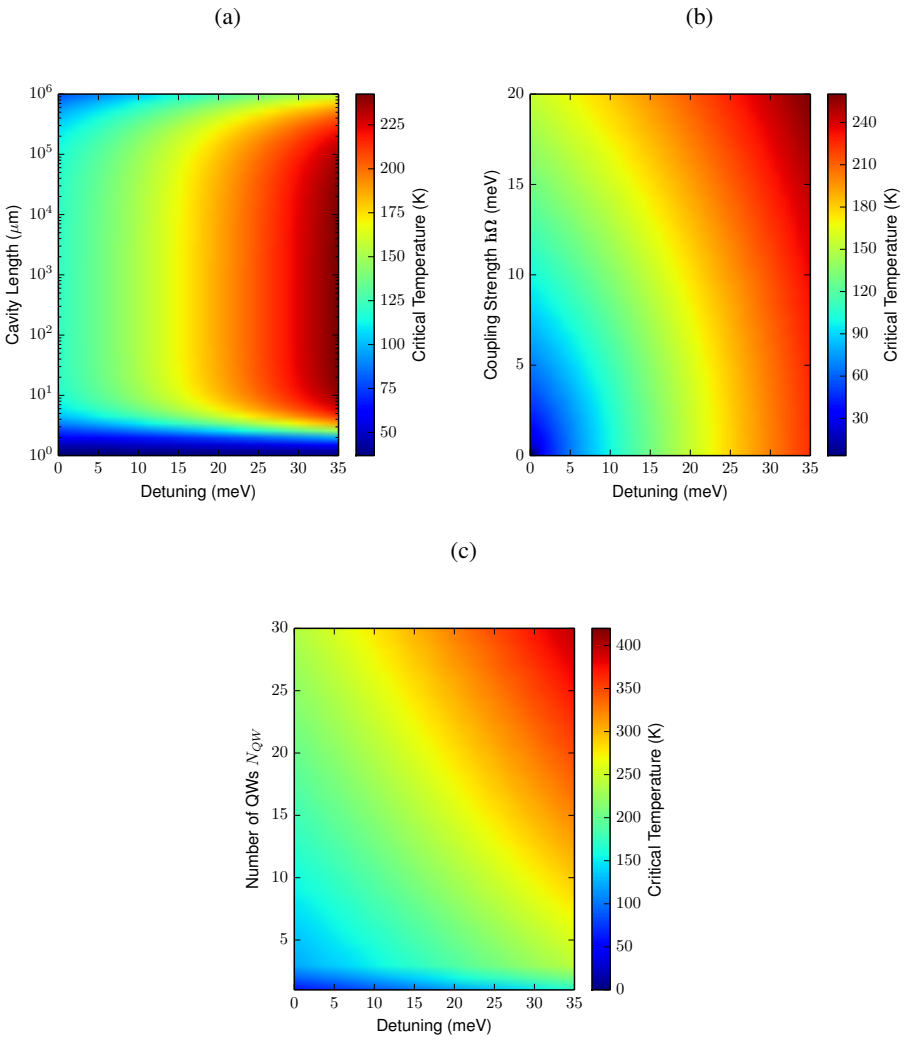

Fig. 6. The critical temperature for the onset of an exciton-polariton BEC as a function of the detuning Δ and (a) the cavity length, (b) coupling strength and (c) the number of QWs in the system. In (a), we assume that there are three QWs in the central slab layer yielding a coupling strength of $\hbar\Omega = 13.7$ meV. In (b) and (c), the cavity length is taken to be $50\,\mu$m. In all cases, the polariton density per QW is $(6.2a_B)^{-2} = 260\,\mu\text{m}^{-2}$ where a_B is the exciton Bohr radius.

#260856 Received 17 Mar 2016; revised 13 May 2016; accepted 8 Jun 2016; published 14 Jun 2016

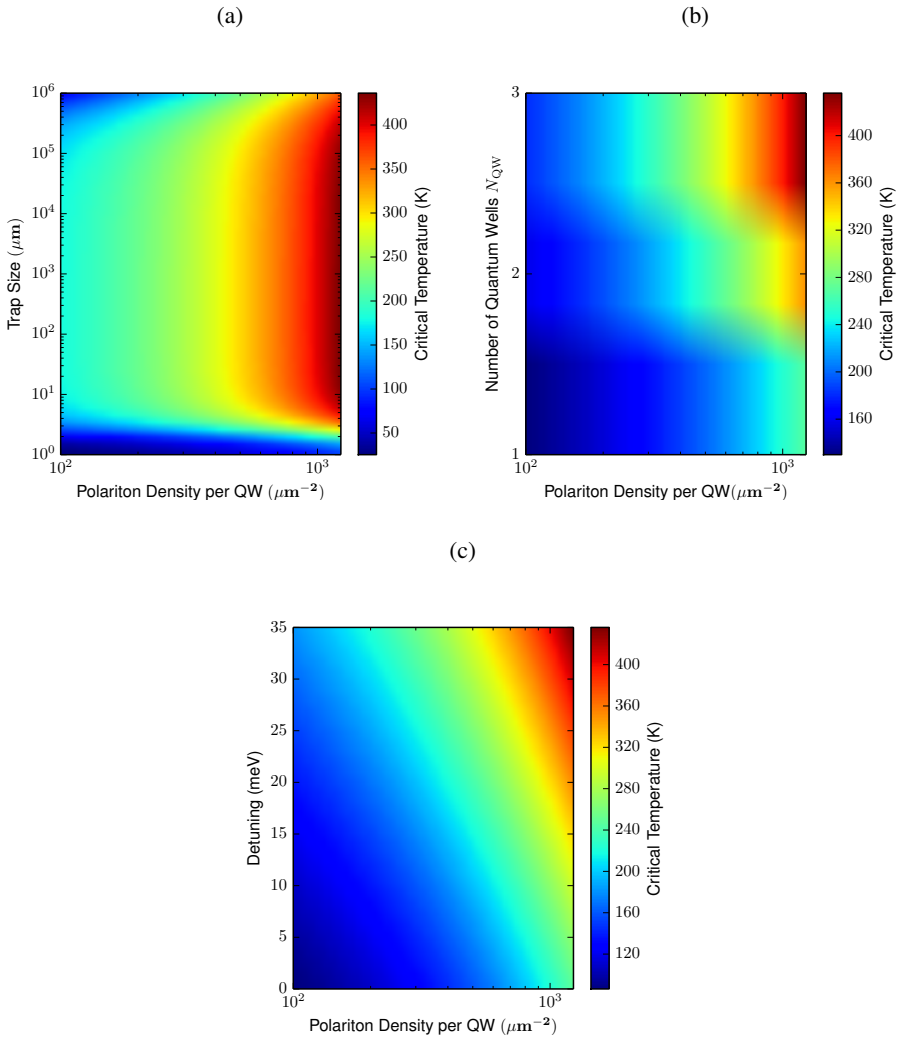

Fig. 7. The BEC critical temperature as a function of the polariton density and (a) cavity length, (b) number of QWs in the system and (c) detuning. In (a), we consider three QWs in the central slab layer yielding a collective coupling strength of $\hbar\Omega = 13.7$ meV and a detuning of $\Delta = 35$ meV. In (b), we consider a cavity length of $D = 50\,\mu\mathrm{m}^{-2}$ and a detuning of $\Delta = 35$ meV. In (c), we consider a cavity length of $D = 50\,\mu\mathrm{m}^{-2}$ and three quantum wells in the central slab layer ($\hbar\Omega = 13.7$ meV). The maximum polariton density per QW is chosen to be $(2.8a_B)^{-2} = 1.2\times10^3\,\mu\mathrm{m}^{-2}$.

#260856 Received 17 Mar 2016; revised 13 May 2016; accepted 8 Jun 2016; published 14 Jun 2016

(average) pore radius of $r_p = 0.305a = 157\,\text{nm}$. For each pore radius, we assume that there are three QWs in the central slab layer. We first compute the remaining photonic band gap between the LP and the lower 3D band edge, relative to the central band gap frequency. As shown in Fig. 8(a), the lower 3D band edge rises in frequency more rapidly with pore radius than the lowest 2D guided mode. Though the remaining PBG remains above 9% for each pore radius considered, the actual PBG in the presence of disorder is the intersection set of all PBGs generated by each of the pore radii. This actual PBG, indicated by the shaded area in Fig. 8(b), remains 9.8% relative to the center frequency (887 meV). This suggests that up to a $\pm 3\%$ variation in pore radius, the LP remains within the band gap and is protected from radiative decay. The detuning Δ, the coupling strength $\hbar\Omega$ and the dispersion depth V for each of the pore radii are depicted in Figs. 8(c) and 8(d). Despite the increase in detuning with decreasing pore radius, the exciton fraction per QW of the LP is still 1% for a pore radius of $r_p = 0.296a = 152$ nm. At this pore radius, the polariton-phonon scattering time is 50 ps. This is still below the exciton non-radiative decay time of 200 ps [40], suggesting that exciton-polaritons can fully thermalize with the host lattice. By choosing the lattice constant $a = 516$ nm, to enforce a detuning of $\Delta = 35$ meV at a pore radius of $0.305a$, the dispersion depth V falls slightly below $k_bT = 26$ meV (for $T = 300$K) for a $\pm 3\%$ variation in pore radius, as shown by the lower blue curve in Fig. 8(d). However, additional robustness to pore radius variations can be obtained by setting the lattice constant to $a = 519$ nm. This sets the detuning to $\Delta = 40$ meV for a pore radius of 0.305a and ensures that the dispersion depth V remains above 26 meV for a $\pm 3\%$ variation in the pore radius about $r_p = 0.305a$, as shown by the upper green curve in Fig. 8(d). Together, our results suggest that equilibrium room-temperature BEC of exciton-polaritons is robust to photonic structure variation of $\pm 3\%$.

We also consider the effect of electronic-scale structural disorder in the QWs, in the form of small random variations in the QW width. This leads to variations in the excitonic energy in each QW. This inhomogeneous broadening is modeled by adding a fluctuation term ΔE_l to the exciton energy in the l^{th} QW: $E_{\text{exc}}^{(l)}(\mathbf{k}) = E_0 + \frac{\hbar^2}{2m_{\text{exc}}}k^2 + \Delta E_l$. We model ΔE_l as a Gaussian random variable with zero mean and a root mean square fluctuation $\Delta E_{\text{rms}} \equiv \left[\overline{(\Delta E_l)^2}\right]^{1/2}$ as large as 10 meV. For each Gaussian distribution, we consider 10^5 random configurations and we compute the standard deviation of the vacuum Rabi splitting, the dispersion depth V and the critical temperature T_c. We assume there are three QWs in a $0.07a$ central slab layer sandwiched by slanted pore photonic crystals with lattice constant $a = 516$ nm and a pore radius of $0.305a$, yielding a detuning of $\Delta = 35$ meV in the absence of any disorder. For the calculation of T_c, we assume a box trap with a side length of $D = 50\,\mu\text{m}$ and a polariton density per QW of $(2.8a_B)^{-2}$.

Fluctuations in the vacuum Rabi splitting arising from electronic disorder are shown in Fig. 9(a). The excitonic energy in the l^{th} QW enters into the exciton-polariton coupling strength in the l^{th} QW, $\tilde{\Omega}_{l,\alpha,n,p,\mathbf{k}}$, in Eq. (3). With only three QWs, the random fluctuations in $\tilde{\Omega}_{l,\alpha,n,p,\mathbf{k}}$ remain important when performing the sum in (7b) and the variance in the vacuum Rabi splitting increases with increasing ΔE_{rms}. The fluctuation in the dispersion depth V also increases with ΔE_{rms} due to random variation of the detuning. The resulting fluctuation in the critical temperature T_c is depicted in Fig. 9(b). Our results suggest that for an inhomogeneous broadening of $\Delta E_{\text{rms}} = 10$ meV, the critical temperature fluctuates by 27 K about the value of 436 K. In other words, room temperature BEC in our system is robust to substantial amounts of structural disorder.

We consider the effect of homogeneous broadening of the exciton linewidth on the critical temperature T_c. The QW exciton is homogeneously broadened due to scattering with longitudinal optical phonons. This mechanism also enables thermal equilibrium with the host lat-

#260856 Received 17 Mar 2016; revised 13 May 2016; accepted 8 Jun 2016; published 14 Jun 2016

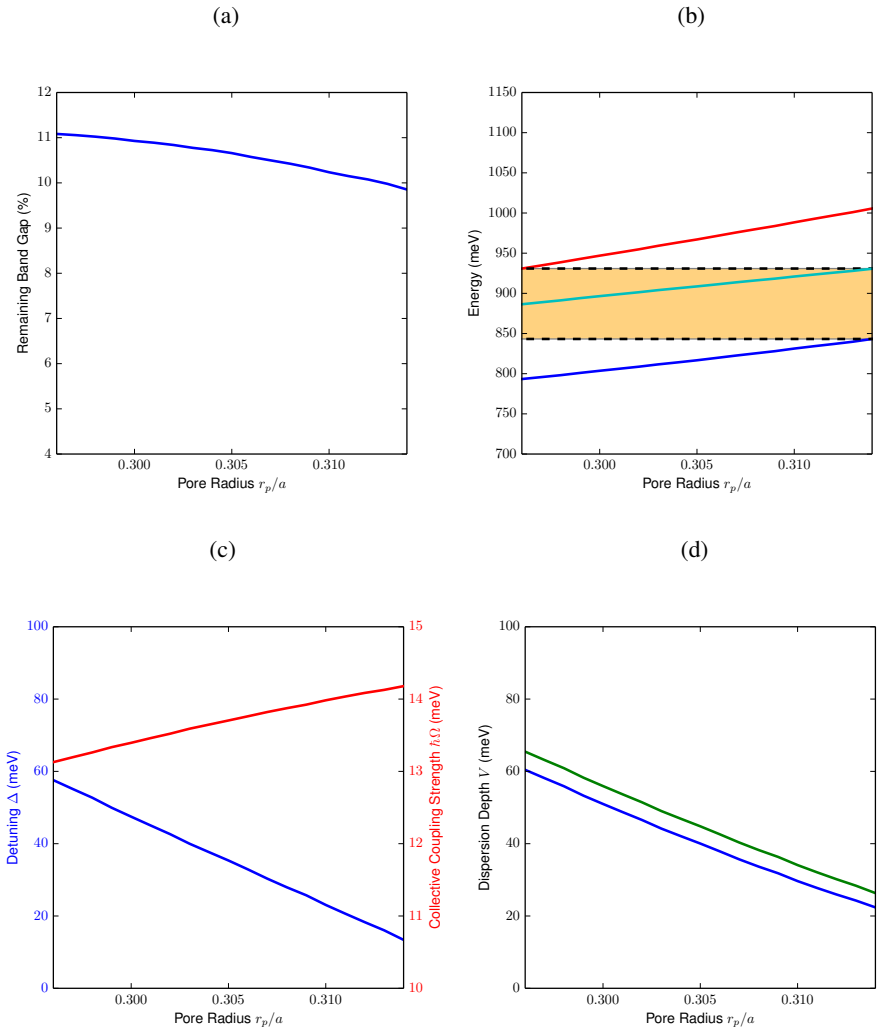

Fig. 8. (a) The remaining PBG between the LP and the lower 3D band edge, relative to the central band gap frequency versus pore radius r_p in the slanted pore photonic crystal. (b) The upper 3D band edge (upper red curve), the lower 3D band edge (lower blue curve) and the LP ground state (middle cyan curve) energies versus pore radius r_p. The shaded area represents the intersection set of photonic band gaps generated by each pore radius. (c) The detuning Δ (blue curve) and the collective coupling strength $\hbar\Omega$ (red curve) and (d) the dispersion depth V versus the pore radius r_p. In all cases, there are three InGaAs/InP QWs embedded in a $0.07a = 36$ nm thick central slab layer layer. In Figs. 8(a), 8(b) and 8(c), the lattice constant is held at $a = 516$ nm to enforce a detuning of $\Delta = 35$ meV when the pore radius is $r_p = 0.305a = 157$ nm. In Fig. 8(d), the lattice constant is $a = 516$ nm (lower blue curve) and $a = 519$ nm (upper green curve) to enforce detunings of $\Delta = 35$ meV and $\Delta = 40$ meV, respectively, when the pore radius is $0.305a$.

#260856 Received 17 Mar 2016; revised 13 May 2016; accepted 8 Jun 2016; published 14 Jun 2016

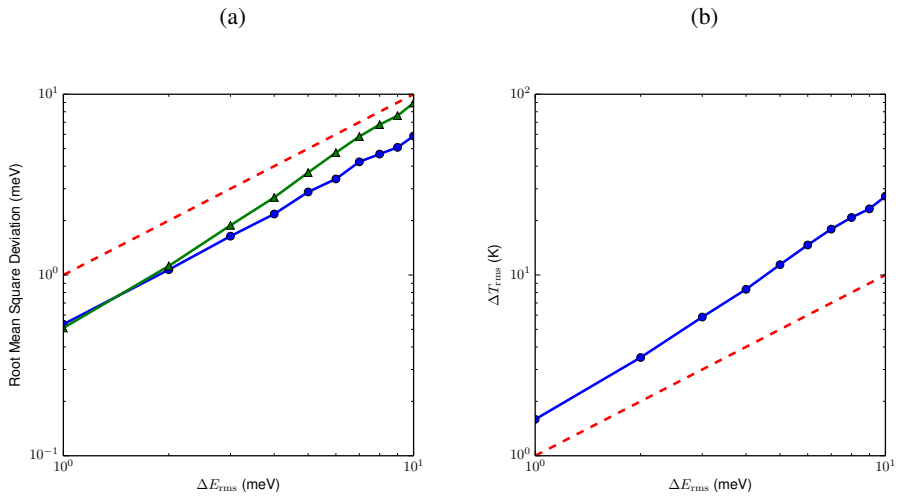

Fig. 9. (a) The root mean square deviation of the dispersion depth V (circles) and the vacuum Rabi splitting $\sqrt{\Delta^2+4\hbar^2\Omega^2}$ (triangles) as a function of the exciton inhomogeneous broadening $\Delta E_{\rm rms}$. (b) The root mean square deviation of the critical temperature T_c as a function of the exciton inhomogeneous broadening $\Delta E_{\rm rms}$. The red dashed line indicates the value of $\Delta E_{\rm rms}$.

tice [75, 76]. A simplified treatment of homogeneous broadening [77] involves adding a term $-i\Gamma$ to the exciton energy $E_{\rm exc}(\mathbf{k})$ in Eq. (4). In this case, the vacuum Rabi splitting (at zero detuning $\Delta = 0$) becomes $\sqrt{4\hbar\Omega^2-\Gamma^2}$. The dispersion depth is given by [45]

$$V = \Delta/2 + \mathrm{Re}\left[(\Delta - i\Gamma)^2 + 4\hbar^2\Omega^2\right]^{1/2}/2. \tag{12}$$

Refs. [45, 75, 76] estimate $\Gamma = 5.4$ meV at room temperature for InGaAs QWs. Accounting for this homogeneous broadening reduces the dispersion depth by approximately 1 meV (with a detuning of $\Delta = 35$ meV and a light-matter coupling strength of $\hbar\Omega = 13.7$ meV) to 39 meV. This dispersion depth can equivalently be obtained (in the absence of homogeneous broadening) by reducing the detuning Δ to 34 meV. As shown in Figs. 6 and 7, this has a minor effect on the critical temperature. Once again, the large positive detuning ensures that room temperature exciton-polariton BEC is robust to excitonic homogeneous broadening.

6. Conclusion

In summary, we have identified a slanted-pore photonic crystal structure sandwiching a planar central slab layer containing three InGaAs/InP QWs in which an equilibrium, room-temperature BEC of exciton-polaritons at near telecommunication frequencies can be obtained. The full three-dimensional photonic band gap (PBG) exhibited by the slanted pore crystals allows for strong light localization in the central active layer, facilitating strong coupling between excitons and planar guided photons within the 3D PBG. This strong light-matter coupling results in coherent, reversible exciton radiative recombination and normal mode splitting into lower and upper polariton branches. The full 3D PBG strongly inhibits the radiative decay of the lower polaritons into extraneous optical modes that can escape the system. This increases their lifetime

#260856 Received 17 Mar 2016; revised 13 May 2016; accepted 8 Jun 2016; published 14 Jun 2016

up to the nonradiative decay timescale, allowing the polariton gas to reach thermal equilibrium with the host lattice, by polariton-phonon scattering.

A high critical temperature for the onset of exciton-polariton BEC is obtained using a two-fold strategy. The first is through the doubling of the polariton density available for BEC. This is achieved in the slanted pore architecture which breaks the x-y polarization degeneracy of polaritons in the quantum well region. This causes all polaritons created to equilibrate near a single wave-vector mode rather than dividing between two degenerate states. The second strategy is to increase the dispersion depth of the resulting non-degenerate lower-polariton branch by detuning the exciton recombination energy above the photonic cavity mode (positive detuning Δ). This leads to a lower polariton with a relatively small excitonic component, but sufficiently large to achieve rapid thermalization. We consider QWs composed of 3 nm InGaAs wells surrounded by 7 nm InP barriers as to allow for the emission of light at a wavelength of 1313 nm. Using three QWs in a 36 nm central slab layer surrounded by slanted pore photonic crystals with a 157 nm pore radius, we achieve a collective coupling strength of $\hbar\Omega = 13.7$ meV. A lower polariton dispersion depth of 40 meV (remaining entirely within the 3D PBG) is obtained using a detuning of $\Delta = 35$ meV. Efficient polariton thermalization via polariton-phonon scattering is still possible.

We identify the optimal parameters in our proposed structure to obtain thermal equilibrium room-temperature exciton-polariton BEC. For a $0.07a$ central slab layer surrounded by slanted pores of radius $0.305a$, a choice of $a = 516$ nm sets the detuning at $\Delta = 35$ meV. Considering a box trap for the polaritons with $D = 50\,\mu$m and a polariton density per quantum well of $(2.8a_B)^{-2} = 1.2 \times 10^3\,\mu\text{m}^{-2}$, we obtain a critical temperature for the onset of an exciton-polariton BEC of 436 K. The bare exciton binding energy in our InGaAs/InP quantum well system is only 7 meV. In the absence of strong-coupling to the photonic cavity mode, the bare exciton would be unstable to dissociation by thermal fluctuations at such high temperature. However, as a result of strong light-matter coupling, the dispersion depth of 40 meV sets the temperature scale of stability of the polariton from thermal dissociation.

We demonstrated the robustness of equilibrium room-temperature exciton-polariton BEC to structural disorder in the photonic crystal and in the QWs. Our study of photonic disorder suggests that room-temperature BEC persists for variations of up to $\pm 3\%$ in the pore radius about the optimal value of $0.305a = 157$ nm. Given the large positive detuning of the exciton from the strong coupled optical mode, we find considerable robustness to inhomogeneous broadening and homogeneous broadening due to longitudinal optical phonon scattering. For an exciton inhomogeneous broadening of 10 meV, the critical temperature fluctuates by only 27 K. For homogeneous broadening of the exciton linewidth by 5.4 meV in InGaAs QWs, the BEC critical temperature remains well above room temperature.

Our proposed structure could have applications as a polariton laser operating near telecommunication frequencies, well above room temeprature. A unique feature of the laser is the thermal equilibrium nature of our condensates. It has been shown [52] that polariton-polariton interactions within the condensate lead to coherence and antibunching of polaritons. This would then be expressed in the quantum statistics of the photons emitted by the laser. A polariton laser using our proposed structure would be "thresholdless," in the sense that there would be no pumping threshold required to replenish radiative losses and to enhance the so-called stimulated scattering of polaritons into the ground state. Due to the emission wavelength of about 1300 nm, it is possible to build such a laser using silicon photonic crystal claddings (instead of InP) sandwiching the InGaAs quantum wells. Given the slightly larger dielectric constant of silicon, the resulting larger 3D photonic band gap would provide even more robustness to the device.

#260856 Received 17 Mar 2016; revised 13 May 2016; accepted 8 Jun 2016; published 14 Jun 2016

Acknowledgments

This work was supported by the United States Department of Energy through Contract No. DE-FG02-06ER46347 and the Natural Sciences and Engineering Research Council of Canada.

#260856 Received 17 Mar 2016; revised 13 May 2016; accepted 8 Jun 2016; published 14 Jun 2016